Monthly Notices
of the
ROYAL ASTRONOMICAL SOCIETY

Mon. Not. R. Astron. Soc. **417,** 2478–2499 (2011) doi:10.1111/j.1365-2966.2011.19411.x

Yarkovsky–O'Keefe–Radzievskii–Paddack effect on tumbling objects

S. Breiter,[1⋆] A. Rożek[1⋆] and D. Vokrouhlický[2⋆]

[1]*Astronomical Observatory, A. Mickiewicz University, Sloneczna 36, PL60-286 Poznań, Poland*
[2]*Institute of Astronomy, Charles University, V Holešovičkách 2, 18000 Prague 8, Czech Republic*

Accepted 2011 July 9. Received 2011 July 8; in original form 2011 May 26

ABSTRACT

A semi-analytical model of the Yarkovsky–O'Keefe–Radzievskii–Paddack (YORP) effect on an asteroid spin in a non-principal axis rotation state is developed. The model describes the spin-state evolution in Deprit–Elipe variables, first-order averaged with respect to rotation and Keplerian orbital motion. Assuming zero conductivity, the YORP torque is represented by spherical harmonic series with vectorial coefficients, allowing us to use any degree and order of approximation. Within the quadrupole approximation of the illumination function we find the same first integrals involving rotational momentum, obliquity and dynamical inertia that were obtained by Cicaló & Scheeres. The integrals do not exist when higher degree terms of the illumination function are included, and then the asymptotic states known from Vokrouhlický et al. appear. This resolves an apparent contradiction between earlier results. Averaged equations of motion admit stable and unstable limit cycle solutions that were not previously detected. Non-averaged numerical integration by the Taylor series method for an exemplary shape of 3103 Eger is in good agreement with the semi-analytical theory.

Key words: radiation mechanisms: thermal – methods: analytical – celestial mechanics – minor planets, asteroids: general.

1 INTRODUCTION

Effects of radiation forces and torques in the long-term orbital and rotational dynamics of small bodies in the Solar system attracted considerable attention during the past decade. Radiation torques, generally dubbed the Yarkovsky–O'Keefe–Radzievskii–Paddack (YORP) effect (Paddack 1969; Rubincam 2000), were proven to secularly accelerate or decelerate the rotation rate and, at the same time, change the obliquity value. Both effects are important enough for <30 km size asteroids with planetary application that recently flourished to a large palette. YORP can tilt the rotation pole of asteroids to preferred directions (Vokrouhlický, Nesvorný & Bottke 2003); in concert with the thermal forces it can move small asteroids in asteroid families to extreme heliocentric distances (Vokrouhlický et al. 2006), relax the distribution of the rotational rate value of a small asteroid to be approximately uniform (Pravec et al. 2008), bring the rotation state to the fission limit and produce binary asteroids (e.g. Walsh, Richardson & Michel 2008) or asteroid pairs (e.g. Pravec et al. 2010). The YORP-driven change of the rotation rate of small near-Earth asteroids has recently been measured directly (Kaasalainen et al. 2007; Lowry et al. 2007; Taylor et al. 2007; Ďurech et al. 2008, 2011).

In spite of many important applications, the YORP theory is still at the beginning of its true advancements. For instance, the comparison of the detected and predicted values of YORP strength is not always perfect. It has been recognized that this might be due to a large sensitivity on small-scale irregularities of the shape (e.g. Breiter et al. 2009; Statler 2009) or inhomogeneity in the density distribution (Scheeres & Gaskell 2008). However, even a larger caveat of the modelling has been mostly avoided so far. This is because – apart from rare exceptions – the YORP effect has been analysed under the simplifying assumption of the principal axis rotation.[1] Yet, this is clearly an inconsistent element in the theory because YORP, with its ability to decelerate the rotation rate, cannot indefinitely maintain rotation about the principal axis. A slightest perturbation would naturally trigger the tumbling state. Moreover, many small (kilometer-size) asteroids arise as products from fragmentation of larger bodies during family-forming events. It is natural to assume that the initial rotation state of these bodies would correspond to a general, tumbling situation. The effects of the internal dissipation (e.g. Sharma, Burns & Hui 2005 and references therein) would bring the rotation close to the principal axis mode. But this is a long, asymptotic process, and certainly the action of YORP is not suspended until its end.

⋆E-mail: breiter@amu.edu.pl (SB); a.rozek@almukantarat.pl (AR); vokrouhl@cesnet.cz (DV)

[1] Whenever the principal axis rotation is mentioned, we mean rotation around the axis of maximum inertia, i.e. the minimum energy state.

Having said that, we see that it is crucial to understand the dynamical outcome of the YORP effect within the model that is not a priori restricted to the simplistic assumption of the principal axis rotation. So far, only two papers dealt with the YORP effect on bodies with a general rotation state; each of them addressed the problem with a different approach and thus suffered different limitations. Vokrouhlický et al. (2007) used a fully numerical scheme. The main result of their work was the description of new asymptotic states of the pure-YORP evolution that were characterized by (i) tumbling, (ii) infinite increase of the rotational angular momentum and (iii) obliquity trapped close to 55° or 125°. These states presumably generalize the previously described asymptotic states in the principal axis rotation theory where the angular momentum either increased without limits or decreased to zero, and obliquity tended to 0, 90° or 180°. Zero angular momentum is obviously not a final state in Vokrouhlický et al. (2007) work because before reaching it, the body starts tumbling and always resets on to the angular momentum gain path. While bringing interesting results, this work had certain drawbacks. First, as any numerical approach, it could only investigate a limited sample of initial conditions and free parameters. Secondly, it relied on some particular discretization of differential equations which might bring delicate issues of systematic trends due to truncation and roundoff errors.

A different route to analyse YORP effects for a body in a general rotation state has been undertaken by Cicaló & Scheeres (2010). These authors used a semi-analytical approach. In particular, they considered perturbed motion of a free top in a general rotation state and analytically averaged the perturbation due to the thermal torques over precession and nutation cycles. En route, they made a simplifying restriction of the illumination function to the second degree representation in cosine of the zenith angle (Cicaló & Scheeres 2010, Section 2.4), which then led to a near-integrability of the problem. While elegant, their solution contradicted numerical results of Vokrouhlický et al. (2007) by indicating a simple circulation of the solution about stable points and only an oscillatory behaviour of the rotational angular momentum. As shown below, Cicaló & Scheeres (2010) rightly guessed that the disagreement may stem from their simplifying assumption about the illumination function, but with their approach they were not able to prove it.

In this work, we extend the path paved by Cicaló & Scheeres (2010) and develop a semi-analytical theory of a free top in the general rotation state perturbed by the YORP torque. Importantly, we remove the simplifying approximation of Cicaló & Scheeres (2010) and represent the illumination function up to any degree of accuracy. Our work is facilitated by using more appropriate Legendre series representation of the illumination function (as opposed to the power series in cosine of the zenith angle) and by representing the unperturbed rotation state in terms of Deprit–Elipe canonical variables instead of Euler angles. Both elements facilitate the analytical averaging technique.

Our new solution corroborates the results of Vokrouhlický et al. (2007) and explains the reasons of its disagreement with Cicaló & Scheeres (2010) by revealing the peculiar nature of the quadrupole YORP approximation.

2 PRELIMINARIES

Special functions and (occasionally nonstandard) notation used in this paper are described in Appendix A.

2.1 Reference frames

Three reference frames will be used in our considerations. All of them have the common origin at the centre of mass of a minor body, and each one is associated with some orthogonal, right-handed basis.

The *orbital frame* is described in terms of the basis $\mathcal{S} = (\hat{\mathbf{s}}_1, \hat{\mathbf{s}}_2, \hat{\mathbf{s}}_3)$. Assuming that the body moves on a heliocentric Keplerian ellipse with the semi-axis a_s and eccentricity e_s, we direct the unit vector $\hat{\mathbf{s}}_1$ from the body centre to the pericentre of the bodycentric Sun orbit. Choosing $\hat{\mathbf{s}}_3$ to be the unit vector of the orbital angular momentum and $\hat{\mathbf{s}}_2 = \hat{\mathbf{s}}_3 \times \hat{\mathbf{s}}_1$, we obtain the frame where the direction of the Sun is determined by

$$\hat{\boldsymbol{r}}_\mathrm{s} = \cos f_\mathrm{s}\, \hat{\mathbf{s}}_1 + \sin f_\mathrm{s}\, \hat{\mathbf{s}}_2. \tag{1}$$

The true anomaly f_s in this frame has the same value as the heliocentric true anomaly of the body at the same epoch.

The *momentum frame* is defined by the basis $\mathcal{T} = (\hat{\boldsymbol{t}}_1, \hat{\boldsymbol{t}}_2, \hat{\boldsymbol{t}}_3)$. We begin its definition by specifying $\hat{\boldsymbol{t}}_3$ directed along the spin angular momentum $\boldsymbol{G}$. Further we will always use the term angular momentum in the meaning of spin-related quantity. Then $\hat{\boldsymbol{t}}_1$ will be directed to the ascending node of the plane perpendicular to $\hat{\boldsymbol{t}}_3$ on the orbital plane. More precisely,

$$\hat{\boldsymbol{t}}_1 = \frac{\hat{\mathbf{s}}_3 \times \hat{\boldsymbol{t}}_3}{\sin\varepsilon}. \tag{2}$$

The angle ε, between orbit normal and angular momentum, will be called obliquity. As usual, the remaining vector $\hat{\boldsymbol{t}}_2 = \hat{\boldsymbol{t}}_3 \times \hat{\boldsymbol{t}}_1$.

The *body frame* is defined according to the properties of the mass distribution of the minor body. The basis $\mathcal{B} = (\hat{\boldsymbol{b}}_1, \hat{\boldsymbol{b}}_2, \hat{\boldsymbol{b}}_3)$ is such that the tensor of inertia expressed in it is a diagonal matrix:

$$\mathbf{I} = \mathrm{diag}(I_1, I_2, I_3), \tag{3}$$

with $I_1 \le I_2 \le I_3$.

2.2 Variables and equations of motion

The Serret–Andoyer variables, commonly used in the Hamiltonian problems, are the set of three angle-type coordinates (ℓ, g and h) and their conjugate momenta L, G and H. If $\boldsymbol{G}$ is the angular momentum vector of a rotating body, then

$$G = ||\boldsymbol{G}||, \qquad L = \boldsymbol{G}\cdot\hat{\boldsymbol{b}}_3 = G\cos J, \qquad H = \boldsymbol{G}\cdot\hat{\boldsymbol{s}}_3 = G\cos\varepsilon. \tag{4}$$

Angle h is measured from $\hat{\boldsymbol{s}}_1$ to $\hat{\boldsymbol{t}}_1$, so that

$$\sin h = \hat{\boldsymbol{s}}_3\cdot(\hat{\boldsymbol{s}}_1\times\hat{\boldsymbol{t}}_1), \qquad \cos h = \hat{\boldsymbol{s}}_1\cdot\hat{\boldsymbol{t}}_1. \tag{5}$$

For the definition of angles g and l, we introduce a unit vector $\hat{\boldsymbol{j}}$ directed to the ascending node of the equator (a plane perpendicular to $\hat{\boldsymbol{b}}_3$) on the plane perpendicular to $\hat{\boldsymbol{t}}_3$ (so-called invariant plane):

$$\hat{\boldsymbol{j}} = \frac{\hat{\boldsymbol{t}}_3\times\hat{\boldsymbol{b}}_3}{\sin J}. \tag{6}$$

Then,

$$\sin g = \hat{\boldsymbol{t}}_3\cdot(\hat{\boldsymbol{t}}_1\times\hat{\boldsymbol{j}}), \qquad \cos g = \hat{\boldsymbol{t}}_1\cdot\hat{\boldsymbol{j}}, \tag{7}$$

and

$$\sin l = \hat{\boldsymbol{b}}_3\cdot(\hat{\boldsymbol{j}}\times\hat{\boldsymbol{b}}_1), \qquad \cos l = \hat{\boldsymbol{j}}\cdot\hat{\boldsymbol{b}}_1. \tag{8}$$

It means that the set (g, J, l) is actually the usual 3-1-3 Euler angles sequence for the transformation from $\mathcal{T}$ to $\mathcal{B}$, often called precession, nutation and intrinsic rotation angles, respectively. For any vector

$$\boldsymbol{u} = u_1\hat{\boldsymbol{s}}_1 + u_2\hat{\boldsymbol{s}}_2 + u_3\hat{\boldsymbol{s}}_3 = u_1'\hat{\boldsymbol{b}}_1 + u_2'\hat{\boldsymbol{b}}_2 + u_3'\hat{\boldsymbol{b}}_3, \tag{9}$$

the coordinates transform according to

$$\begin{pmatrix} u_1' \\ u_2' \\ u_3' \end{pmatrix} = \mathbf{R}(g, J, l)\,\mathbf{R}_1(\varepsilon)\,\mathbf{R}_3(h)\begin{pmatrix} u_1 \\ u_2 \\ u_3 \end{pmatrix}, \tag{10}$$

where the matrix $\mathbf{R}(g, J, l) = \mathbf{R}_3(l)\mathbf{R}_1(J)\,\mathbf{R}_3(g)$ describes the passive rotation from $\mathcal{T}$ to $\mathcal{B}$.

The Euler–Poinsot problem of the free top is defined by the Hamiltonian function

$$\mathcal{H} = \frac{1}{2}\boldsymbol{\Omega}\cdot\boldsymbol{G} = \frac{1}{2}\left(a_1\sin^2 l + a_2\cos^2 l\right)(G^2 - L^2) + \frac{a_3}{2}L^2, \tag{11}$$

equal to the kinetic energy of rotation. Following Deprit & Elipe (1993) we use the inverses of principal moments of inertia

$$a_j = I_j^{-1}, \qquad a_3 \le a_2 \le a_1, \tag{12}$$

as the convenient parameters. The angular velocity vector $\boldsymbol{\Omega}$ is the product of the inverse matrix of inertia $\mathbf{I}^{-1}$ and angular momentum $\boldsymbol{G}$. Their coordinates in the body frame $\mathcal{B}$ are linked by the simple relations

$$\boldsymbol{\Omega}\cdot\hat{\boldsymbol{b}}_j = a_j\,\boldsymbol{G}\cdot\hat{\boldsymbol{b}}_j, \quad j = 1, 2, 3. \tag{13}$$

Canonical equations derived from $\mathcal{H}$ imply that in the motion of the free top h, H and G (hence ε) are constant, whereas l, g and L (hence J) are the nonlinear functions of time. Two different sets of canonical reduction leading to three constant momenta were proposed: Sadov (1970) and Kinoshita (1972) found angle-action variables solving the Hamilton–Jacobi equation, whereas Deprit & Elipe (1993) took a different approach based upon geometrical insight. The variables of Deprit and Elipe consist of three coordinates: δ is a quantity having the dimension of angular velocity, while γ and h are the angles. Their conjugate momenta are Δ, Γ and H. The (h, H) pair is the same as in the Serret–Andoyer set. The momentum $\Gamma = ||\boldsymbol{G}||$, so in the following discussion we will simply use the symbol G. The meaning of Δ is clear from the form of the new Hamiltonian $\mathcal{K}$:

$$\mathcal{K} = \frac{G^2}{2\Delta}. \tag{14}$$

The variable occurs to be the dynamical inertia $\Delta = G^2/(2\mathcal{K})$, playing the important role in rigid body problems.

From the point of view of qualitative features in the evolution of a minor body rotation, we are mostly interested in the three momenta of the Deprit–Elipe variables Δ, G and H because they carry the most important information about the total angular momentum (G), inclination of angular momentum axis to the orbital plane (G and H define ε), rotation type and extreme values of the nutation angle J (Δ). In the presence of an arbitrary torque $\boldsymbol{M}$ the evolution of these variables is governed by the following equations:

$$\dot{\Delta} = \frac{2\Delta}{G}\left(\hat{\boldsymbol{t}}_3\cdot\boldsymbol{M} - \frac{\Delta}{G}\,\boldsymbol{\Omega}\cdot\boldsymbol{M}\right), \tag{15}$$

$$\dot{G} = \hat{\boldsymbol{t}}_3\cdot\boldsymbol{M}, \tag{16}$$

$$\dot{H} = \hat{\boldsymbol{s}}_3\cdot\boldsymbol{M}. \tag{17}$$

Although equation (17) looks apparently simple, it is easier to use instead an equation for $\dot{\varepsilon} = -(\dot{H} - \cos\varepsilon\,\dot{G})/(G\sin\varepsilon)$, having a basis independent form

$$\dot{\varepsilon} = -\frac{\hat{\boldsymbol{t}}_2 \cdot \boldsymbol{M}}{G}. \tag{18}$$

In principle, this set is equivalent to the one used by Cicaló & Scheeres (2010), who used symbols L, δ and I_D for our present G, ε and Δ. Numerical integration results presented by Vokrouhlický et al. (2007) were also discussed in terms of G, ε and $p = 1/(a_2\Delta)$.

Explicit relations between $(\gamma,\ \delta)$ and $(g,\ l)$ are fairly complicated (Deprit & Elipe 1993; Gurfil et al. 2007). Our variant of these expressions is given in Appendix B.

3 YORP TORQUE

Let us impose the following assumptions: a minor body is homogeneous, its thermal conductivity is null, and the body surface scatters incident radiation from the Sun (located at $\boldsymbol{r}_\mathrm{s}$ and moving on the ellipse with the semi-axis a_s) according to the Lambert law and re-emits it thermally like a grey body. Then, the definition of the YORP torque is

$$\boldsymbol{M} = -\frac{\kappa}{V}\left(\frac{a_\mathrm{s}}{r_\mathrm{s}}\right)^2 \oint \nu(\hat{\boldsymbol{n}}, \hat{\boldsymbol{r}}_\mathrm{s})\, \boldsymbol{r}\times\hat{\boldsymbol{n}}\,\mathrm{d}S. \tag{19}$$

We use the body volume

$$V = \int \mathrm{d}V = \frac{1}{3}\oint \boldsymbol{r}\cdot\hat{\boldsymbol{n}}\,\mathrm{d}S \tag{20}$$

as a normalizing factor, so that κ, defined as

$$\kappa = \frac{2}{3}\frac{V\,\Phi_0}{c}\left(\frac{d_0}{a_\mathrm{s}}\right)^2, \tag{21}$$

has the same unit as $\boldsymbol{M}$, leaving the remaining subexpression dimensionless. Equation (21) involves the velocity of light c, and the solar constant Φ_0, i.e. the radiant flux at the nominal distance of $d_0 = 1$ au.

Convex bodies admit the simplest form of the illumination factor ν, a function of unit outward normal to the surface $\hat{\boldsymbol{n}}$ and the solar direction $\hat{\boldsymbol{r}}_\mathrm{s}$, namely

$$\nu(\hat{\boldsymbol{n}}, \hat{\boldsymbol{r}}_\mathrm{s}) = \max(0,\ \hat{\boldsymbol{n}}\cdot\hat{\boldsymbol{r}}_\mathrm{s}) \tag{22}$$

because no shadows are cast by one surface element on another. Mysen (2008) and Cicaló & Scheeres (2010) approximate ν using either truncated Fourier series of the Sun's zenith distance z_s or its conversion to the polynomial of $\cos z_\mathrm{s} = \hat{\boldsymbol{n}}\cdot\hat{\boldsymbol{r}}_\mathrm{s}$. The former is not well adapted to further analytical treatment, whereas the latter requires the replacement of all coefficients when changing the maximum degree of the polynomial. In our opinion, the best choice is to use the expansion of ν in the Legendre series:

$$\nu(\hat{\boldsymbol{n}}, \hat{\boldsymbol{r}}_\mathrm{s}) = \sum_{n\ge 0} c_n\, P_n(\hat{\boldsymbol{n}}\cdot\hat{\boldsymbol{r}}_\mathrm{s}), \tag{23}$$

where the coefficients are given by simple quadratures

$$c_n = \frac{2n+1}{2}\int_{-1}^{1}\max(0,x)\,P_n(x)\,\mathrm{d}x = \frac{2n+1}{2}\int_0^1 x\,P_n(x)\,\mathrm{d}x, \tag{24}$$

leading to

$$c_0 = \frac{1}{4},\qquad c_1 = \frac{1}{2},\qquad c_2 = \frac{5}{16},\qquad c_3 = 0,\qquad c_4 = -\frac{3}{32}, \tag{25}$$

and generally, for all $n \ge 1$,

$$c_{2n+1} = 0,\qquad c_{2n} = -\frac{(2n-3)(4n+1)}{(2n+2)(4n-3)}\,c_{2n-2} = -\frac{(4n+1)\,P_{2n}(0)}{(4n+4)\,(2n-1)}. \tag{26}$$

Expressing the YORP torque as the Legendre series,

$$\boldsymbol{M} = -\frac{\kappa}{V}\left(\frac{a_\mathrm{s}}{r_\mathrm{s}}\right)^2 \sum_{n\ge 0} c_n \oint P_n(\hat{\boldsymbol{n}}\cdot\hat{\boldsymbol{r}}_\mathrm{s})\,\boldsymbol{r}\times\hat{\boldsymbol{n}}\,\mathrm{d}S, \tag{27}$$

we can separate the position of the Sun from the body-shape-related quantities by applying the addition theorem (A17). This, however, requires some choice of basis. The body frame has a definite advantage of leading to constant values of surface integral, so encapsulating the body shape contribution in dimensionless vectorial coefficients $\boldsymbol{v}_{n,m} \in \mathbb{C}^3$, defined as

$$\boldsymbol{v}_{n,m} = \frac{4\pi}{2n+1}\frac{c_n}{V}\oint Y^*_{n,m}(\hat{\boldsymbol{n}}|\mathcal{B})\,\boldsymbol{r}\times\hat{\boldsymbol{n}}\,\mathrm{d}S, \tag{28}$$

we finally obtain

$$\boldsymbol{M} = -\kappa\left(\frac{a_\mathrm{s}}{r_\mathrm{s}}\right)^2 \sum_{n\ge 1}\sum_{m=-n}^{n} \boldsymbol{v}_{n,m} Y_{n,m}(\hat{\boldsymbol{r}}_\mathrm{s}|\mathcal{B}). \tag{29}$$

Although formally $\boldsymbol{M}$ may stand for the YORP torque in any coordinate system, it is most convenient to use the body frame $\mathcal{B}$ where the vector coefficients $\boldsymbol{v}_{n,m}$ are constant. Actually, equation (29) is a complex version of the real (sine/cosine) series postulated by Scheeres & Mirrahimi (2008). For a polyhedral model of an object, the surface integral in (28) is replaced by a simple sum over planar faces.

The sum in equation (29) begins with $n = 1$, because $\boldsymbol{v}_{0,0} = \boldsymbol{0}$, according to the Gauss theorem (cf. Mysen 2007). It is noteworthy that the general form (29) is not restricted to convex objects or isotropic reflection and radiation models. Vector coefficients $\boldsymbol{v}_{n,m}$ may be computed from the values of the torque sampled on a grid of Sun directions in the body frame using a shadowing algorithm for non-convex objects and more elaborate reflection and emission laws (Statler 2009; Breiter, Bartczak & Czekaj 2010; Breiter & Vokrouhlický 2011). Even for the purpose of numerical integration, the series (29) may have some advantage, because they are $\mathcal{C}^\infty$ smooth, whereas usual polyhedral models provide the torques that are only $\mathcal{C}^0$ continuous. Discontinuous derivatives may significantly degrade the performance of integrators and even exclude the use of some methods (like the Taylor series).

4 FIRST-ORDER AVERAGING

4.1 Principles

Considered in the body frame, the YORP torque $\boldsymbol{M}$ introduced in the previous section is a function of the direction and distance to the Sun. As such it is explicitly time dependent, being a 2π-periodic function of the mean anomaly l_s. On the other hand, it is also a quasi-periodic function of angles γ and δ – both being the linear functions of time. Deprit–Elipe variables do not form an action-angle set, and free-top motion is not 2π periodic in any of the two angles; yet it does not exclude their application in averaging. We have a choice of either using appropriate periods $P_\gamma(G,\,\Delta)$ and $P_\delta(G,\,\Delta)$ in the averaging operator or replacing the angles with $\overline{g}_j$ and $\overline{\psi}_j$ from Appendix B. Taking the second option and using the Euler–Poinsot problem plus Keplerian orbital motion as the averaging kernel, we remove the periodic terms from the right-hand sides of equations (15), (16) and (18) by means of an iterated integral

$$\langle F\rangle = \frac{1}{(2\pi)^3}\int_0^{2\pi}\int_0^{2\pi}\int_0^{2\pi} F\,\mathrm{d}l_\mathrm{s}\,\mathrm{d}\overline{g}_j\,\mathrm{d}\overline{\psi}_j, \tag{30}$$

where F stands for any of the right-hand sides. This integral is a legitimate equivalent of the time average of F as long as the motion is quasi-periodic, and frequencies associated with the three angles satisfy the irrationality condition.

The first step of our procedure will generate the orbital average $\langle\boldsymbol{M}\rangle_\mathrm{o}$. Since $\hat{\boldsymbol{r}}_\mathrm{s}$ and r_s are expressed in terms of true anomaly f_s, the time average over one orbital period is given by

$$\langle F(f_\mathrm{s})\rangle_\mathrm{o} = \frac{1}{2\pi}\int_0^{2\pi}\frac{r_\mathrm{s}^2 F(f_\mathrm{s})}{a_\mathrm{s}^2\,\eta_\mathrm{s}}\,\mathrm{d}f_\mathrm{s}, \tag{31}$$

where

$$\eta_\mathrm{s} = \sqrt{1-e_\mathrm{s}^2}. \tag{32}$$

The next phase, which we name precession averaging, formally involves integration with respect to $\overline{g}_j$. Yet, our functions F are primarily given it terms of Serret–Andoyer $(l,\,g,\,L,\,G)$ set. With G being constant, and $(l,\,L)$ explicitly expressible in terms of $\overline{\psi}_j$, the only point that may raise some doubts is the form of $g = \overline{g}_j + \Phi(\overline{\psi}_j)$ given in equations (B17) and (B29). But evaluating

$$\langle F\rangle = \frac{1}{4\pi^2}\int_0^{2\pi}\int_0^{2\pi}\langle F\rangle_\mathrm{o}\,\mathrm{d}\overline{g}_j\,\mathrm{d}\overline{\psi}_j, \tag{33}$$

as an iterated integral, we fix the value of $\overline{\psi}_j$ while integrating with respect to $\overline{g}_j$. Hence we may simply replace the mean value with respect to $\overline{g}_j \in [0,\ 2\pi]$ by the mean value with respect to

$$g \in \left[\Phi(\overline{\psi}_j),\ \Phi(\overline{\psi}_j) + 2\pi\right]$$

or – equivalently – to $g \in [0,\ 2\pi]$, since the mean value of a periodic function is independent of such interval shifts. Thus, defining rigorously the double average with respect to the orbital motion and precession as

$$\langle F\rangle_\mathrm{op} = \frac{1}{2\pi}\int_0^{2\pi}\langle F\rangle_\mathrm{o}\,\mathrm{d}g, \tag{34}$$

we will proceed to the final mean value

$$\langle F\rangle = \frac{1}{2\pi}\int_0^{2\pi}\langle F\rangle_\mathrm{op}\,\mathrm{d}\overline{\psi}_j. \tag{35}$$

This step is best performed using the explicit time dependence of $\overline{\psi}_j$ and $(l,\,L)$ given in Appendix B, which requires a separate treatment in the short axis $(j = 3)$ and long axis $(j = 1)$ rotation modes:

$$\langle F\rangle = \frac{1}{4K(k_j)}\int_0^{4K(k_j)}\langle F\rangle_\mathrm{op}\,\mathrm{d}u_j, \tag{36}$$

where $u_j = n_j\,t = 2K(k_j)\overline{\psi}_j/\pi$.

4.2 Orbital averaging

The simplest way to find the mean value of the YORP torque $\langle \boldsymbol{M} \rangle_{\rm o}$ is to make a small detour: instead of averaging equation (29), let us consider equation (27) which is still in a coordinate-free form. Applying rule (31) to the Sun-dependent factor in equation (27) we benefit from the addition theorem (A17), leading to

$$\left\langle \left(\frac{a_{\rm s}}{r_{\rm s}}\right)^2 P_n(\hat{\boldsymbol{n}}\cdot\hat{\boldsymbol{r}}_{\rm s}) \right\rangle_{\rm o} = \frac{2}{(2n+1)\,\eta_{\rm s}} \sum_{m=-n}^{n} Y_{n,m}(\hat{\boldsymbol{n}}|\mathcal{S}) \int_0^{2\pi} Y^*_{nm}(\hat{\boldsymbol{r}}_{\rm s}|\mathcal{S})\,{\rm d}f_{\rm s} = \frac{4\pi}{(2n+1)\,\eta_{\rm s}} Y_{n,0}(\hat{\boldsymbol{n}}|\mathcal{S}) Y^*_{n,0}(\hat{\boldsymbol{r}}_{\rm s}|\mathcal{S}) = \frac{P_n(0)}{\eta_{\rm s}}\, P_n(\hat{\boldsymbol{n}}\cdot\hat{\mathbf{s}}_3). \tag{37}$$

Note that $P_n(0) = 0$ for all odd values of n. Thus, in any frame, the orbital average of the YORP torque is

$$\langle \boldsymbol{M} \rangle_{\rm o} = -\frac{\kappa}{\eta_{\rm s}\, V} \sum_{n\geq 1} c_{2n}\, P_{2n}(0) \oint P_{2n}(\hat{\boldsymbol{n}}\cdot\hat{\mathbf{s}}_3)\, \boldsymbol{r}\times\hat{\boldsymbol{n}}\,{\rm d}S. \tag{38}$$

If we want to separate the contributions of a surface normal $\hat{\boldsymbol{n}}$ and the orbital basis vector $\hat{\mathbf{s}}_3$, we have to choose some basis. Similar to (29), we choose the body frame and use the addition theorem (A17):

$$\langle \boldsymbol{M} \rangle_{\rm o} = -\frac{\kappa}{\eta_{\rm s}\, V} \sum_{n\geq 1} \frac{4\pi}{4n+1}\, c_{2n}\, P_{2n}(0) \sum_{m=-2n}^{2n} Y_{2n,m}(\hat{\mathbf{s}}_3|\mathcal{B}) \oint Y^*_{2n,m}(\hat{\boldsymbol{n}}|\mathcal{B})\, \boldsymbol{r}\times\hat{\boldsymbol{n}}\,{\rm d}S. \tag{39}$$

Thus, defining

$$\boldsymbol{w}_{nm} = \frac{4\pi}{2n+1}\,\frac{c_n\, P_n(0)}{\eta_{\rm s}\, V} \oint Y^*_{n,m}(\hat{\boldsymbol{n}}|\mathcal{B})\, \boldsymbol{r}\times\hat{\boldsymbol{n}}\,{\rm d}S = \frac{P_n(0)}{\eta_{\rm s}}\,\boldsymbol{v}_{nm}, \tag{40}$$

we find the orbital average of the YORP torque in the form analogous to (29):

$$\langle \boldsymbol{M} \rangle_{\rm o} = -\kappa \sum_{n\geq 1} \sum_{m=-2n}^{2n} \boldsymbol{w}_{2n,m}\, Y_{2n,m}(\hat{\mathbf{s}}_3|\mathcal{B}). \tag{41}$$

4.3 Precession angle averaging

The second averaging aims at rejecting purely periodic terms related to the precession frequency according to equation (34). For this purpose we need three building blocks:

$$Q_0 = \left\langle Y_{2n,m}(\hat{\mathbf{s}}_3|\mathcal{B}) \right\rangle_{\rm p} = \frac{1}{2\pi}\int_0^{2\pi} Y_{2n,m}(\hat{\mathbf{s}}_3|\mathcal{B})\,{\rm d}g, \tag{42}$$

$$Q_+ = \left\langle \cos g\, Y_{2n,m}(\hat{\mathbf{s}}_3|\mathcal{B}) \right\rangle_{\rm p}, \tag{43}$$

$$Q_- = \left\langle \sin g\, Y_{2n,m}(\hat{\mathbf{s}}_3|\mathcal{B}) \right\rangle_{\rm p}. \tag{44}$$

The evaluation of Q_0 is straightforward: we move to the basis $\mathcal{T}$, where

$$\hat{\mathbf{s}}_3 = \sin\varepsilon\,\hat{\boldsymbol{t}}_2 + \cos\varepsilon\,\hat{\boldsymbol{t}}_3 \tag{45}$$

is independent of the precession angle g. This involves the rotation of a harmonic according to equation (A12), where $\mathcal{E} = \mathcal{T}$, and $\mathcal{E}' = \mathcal{B}$:

$$Q_0 = \sum_{k=-2n}^{2n} \left\langle D^{2n}_{k,m}(g,J,l)\, Y_{2n,k}(\hat{\mathbf{s}}_3|\mathcal{T}) \right\rangle_{\rm p} = D^{2n}_{0,m}(g,J,l)\, Y_{2n,0}(\hat{\mathbf{s}}_3|\mathcal{T}). \tag{46}$$

By the application of equation (A21) we find

$$Q_0 = Y_{2n,m}(\hat{\boldsymbol{t}}_3|\mathcal{B}) P_{2n}(\hat{\mathbf{s}}_3\cdot\hat{\boldsymbol{t}}_3) = P_{2n}(\cos\varepsilon)\, Y_{2n,m}(\hat{\boldsymbol{t}}_3|\mathcal{B}), \tag{47}$$

which means that the doubly averaged torque in the body frame reads

$$\langle \boldsymbol{M} \rangle_{\rm op} = -\kappa \sum_{n\geq 1} P_{2n}(\cos\varepsilon) \sum_{m=-2n}^{2n} \boldsymbol{w}_{2n,m}\, Y_{2n,m}(\hat{\boldsymbol{t}}_3|\mathcal{B}). \tag{48}$$

Finding Q_+ and Q_- we proceed similarly

$$Q_\pm = \frac{{\rm i}^{(-1\pm1)/2}}{2} \sum_{k=-2n}^{2n} \left\langle \left({\rm e}^{{\rm i}\,g} \pm {\rm e}^{-{\rm i}\,g}\right) D^{2n}_{k,m}(g,J,l)\, Y_{2n,k}(\hat{\mathbf{s}}_3|\mathcal{T}) \right\rangle_{\rm p}, \tag{49}$$

obtaining

$$Q_\pm = \frac{{\rm i}^{(-1\pm1)/2}}{2} \left(D^{2n}_{1,m}(0,J,l)\, Y_{2n,1}(\hat{\mathbf{s}}_3|\mathcal{T}) \pm D^{2n}_{-1,m}(0,J,l)\, Y_{2n,-1}(\hat{\mathbf{s}}_3|\mathcal{T}) \right) = \frac{{\rm i}^{(1\pm1)/2}}{2} \left[D^{2n}_{1,m}(0,J,l) \pm D^{2n}_{-1,m}(0,J,l) \right] \Theta^1_{2n}(\cos\varepsilon). \tag{50}$$

The sum and difference in the square brackets can be expressed in terms of spherical harmonics, leading to

$$Q_+ = {\rm i}\,\frac{\Theta^1_{2n}(\cos\varepsilon)}{2\,\sigma_{2n,-1}} \left(\sigma^+_{2n,m} {\rm e}^{-{\rm i}\,l} Y_{2n,m-1}\left(\hat{\boldsymbol{t}}_3|\,\mathcal{B}\right) + \sigma^-_{2n,m} {\rm e}^{{\rm i}\,l} Y_{2n,m+1}\left(\hat{\boldsymbol{t}}_3|\,\mathcal{B}\right) \right), \tag{51}$$

and

$$Q_- = \frac{\Theta^1_{2n}(\cos\varepsilon)}{2\,\sigma_{2n,-1}\cos J}\,\left(\sigma^+_{2n,m}\mathrm{e}^{-\mathrm{i}l}Y_{2n,m-1}\left(\hat{\boldsymbol{t}}_3|\,\mathcal{B}\right) - \sigma^-_{2n,m}\mathrm{e}^{\mathrm{i}l}Y_{2n,m+1}\left(\hat{\boldsymbol{t}}_3|\,\mathcal{B}\right)\right), \tag{52}$$

where

$$\sigma^{\pm}_{n,m} = \sqrt{(n\pm m)(n\mp m+1)}. \tag{53}$$

So, after the second averaging, we consider the following set of equations of motion:

$$\left\langle\dot{\Delta}\right\rangle_{\rm op} = \frac{2\Delta}{G}\left(\hat{\boldsymbol{t}}_3\cdot\langle\boldsymbol{M}\rangle_{\rm op} - \frac{\Delta}{G}\,\boldsymbol{\Omega}\cdot\langle\boldsymbol{M}\rangle_{\rm op}\right) = -\frac{2\Delta\kappa}{G}\sum_{n\geq1}P_{2n}(\cos\varepsilon)\sum_{m=-2n}^{2n}\left(\hat{\boldsymbol{t}}_3 - \frac{\Delta}{G}\,\boldsymbol{\Omega}\right)\cdot\boldsymbol{w}_{2n,m}\,Y_{2n,m}(\hat{\boldsymbol{t}}_3|\mathcal{B}), \tag{54}$$

$$\left\langle\dot{G}\right\rangle_{\rm op} = \hat{\boldsymbol{t}}_3\cdot\langle\boldsymbol{M}\rangle_{\rm op} = -\kappa\sum_{n\geq1}P_{2n}(\cos\varepsilon)\sum_{m=-2n}^{2n}\left(\hat{\boldsymbol{t}}_3\cdot\boldsymbol{w}_{2n,m}\right)\,Y_{2n,m}(\hat{\boldsymbol{t}}_3|\mathcal{B}), \tag{55}$$

$$\langle\dot{\varepsilon}\rangle_{\rm op} = -\frac{\left\langle\hat{\boldsymbol{t}}_2\cdot\boldsymbol{M}\right\rangle_{\rm op}}{G} = \frac{\kappa}{G}\sum_{n\geq1}\sum_{m=-2n}^{2n}\hat{\boldsymbol{j}}\cdot\boldsymbol{w}_{2n,m}\,Q_- + \left(\hat{\boldsymbol{t}}_3\times\hat{\boldsymbol{j}}\right)\cdot\boldsymbol{w}_{2n,m}\,Q_+. \tag{56}$$

The symbols G, Δ, ε etc. on the right-hand sides have the meaning of doubly averaged mean variables, but we skip the formal labeling like $\langle G\rangle_{\rm op}$ for the sake of brevity.

Note that according to equation (13), there is a simple relation between the vectors appearing in equations (54) and (55)

$$\left(\hat{\boldsymbol{t}}_3 - \frac{\Delta}{G}\,\boldsymbol{\Omega}\right)\cdot\hat{\boldsymbol{b}}_j = (1 - a_j\,\Delta)\,\hat{\boldsymbol{t}}_3\cdot\hat{\boldsymbol{b}}_j, \tag{57}$$

which means that in the last averaging, $\dot{\Delta}$ and $\dot{G}$ should use similar building blocks.

4.4 Nutation and intrinsic rotation angles averaging

4.4.1 Recurrence rules

In the final step we evaluate the mean values with respect to the motion of the angular momentum vector in the body frame. In other word, we are going to suppress the dependence of equations of motion on the nutation angle J and rotation angle l, concluding the path from $Y_{n,m}(\hat{\boldsymbol{r}}_{\rm s}|\mathcal{B})$ through $Y_{n,m}(\hat{\boldsymbol{s}}_3|\mathcal{B})$ and $Y_{n,m}(\hat{\boldsymbol{t}}_3|\mathcal{B})$ to the trivial $Y_{n,m}(\hat{\boldsymbol{b}}_3|\mathcal{B})$. This time, we have to distinguish two cases: the short-axis mode (SAM) of $\boldsymbol{G}$ circulating around $\hat{\boldsymbol{b}}_3$ and the long-axis mode (LAM) of $\boldsymbol{G}$ circulating around $\hat{\boldsymbol{b}}_1$. Appropriate expressions for these two types of motion can be found in Appendix B.

Inspecting definitions of symbols appearing in equations (54)–(56) we may observe that, regardless of the rotation mode, the right-hand sides are polynomials of Jacobian elliptic functions with non-negative exponents. Thus, according to equation (36), the last averaging amounts to evaluating quadratures

$$I^c_{a,b} = \frac{1}{2\,\pi}\int_0^{4K_j}\mathrm{sn}^a\,\mathrm{cn}^b\,\mathrm{dn}^c\,\mathrm{d}u_j. \tag{58}$$

For brevity, we skip the argument u and modulus k_j of elliptic functions [$\mathrm{sn} = \mathrm{sn}(u_j, k_j)$, etc.] and of the complete integral of the first kind $K_j = K(k_j)$, where $j = 1$ for LAM and $j = 3$ for SAM. The mean value of the integrand is related to $I^c_{a,b}$ through a simple relation

$$\left\langle\mathrm{sn}^a\,\mathrm{cn}^b\,\mathrm{dn}^c\right\rangle = \frac{\pi}{2K_j}I^c_{a,b}, \tag{59}$$

where the factor $\pi/(2K_j) = 1$ in the special rotation cases $\hat{\boldsymbol{t}}_3 = \pm\hat{\boldsymbol{b}}_3$ or $\hat{\boldsymbol{t}}_3 = \pm\hat{\boldsymbol{b}}_1$ and decreases towards 0 when $a_2\Delta$ tends to 1.

Elementary symmetry properties of elliptic functions lead to

$$I^c_{2a+1,b} = I^c_{a,2b+1} = 0, \tag{60}$$

and we can focus on even values of a and b exclusively. But since $\mathrm{cn}^{2b} = (1 - \mathrm{sn}^2)^b$, any $I^c_{2a,2b}$ is expressible in terms of $I^c_{2a,0},\ldots,I^c{}_{2(a+b),0}$, by means of the recurrence

$$I^c_{2a,2b} = I^c_{2a,2b-2} - I^c_{2a+2,2b-2}. \tag{61}$$

Moreover, depending on the parity of c, we have

$$\mathrm{dn}^{2c} = (1 - k^2\mathrm{sn}^2)^c \quad\text{or}\quad \mathrm{dn}^{2c+1} = (1 - k^2\mathrm{sn}^2)^c\,\mathrm{dn}, \tag{62}$$

so

$$I^c_{2a,2b} = I^{c-2}_{2a,2b} - k_j^2\,I^{c-2}_{2a+2,2b}. \tag{63}$$

Accordingly, using the starters

$$I^0_{0,0} = \frac{2K_j}{\pi},\qquad I^1_{0,0} = 1,\qquad I^0_{2,0} = \frac{2\,(K_j - E_j)}{\pi\,k_j^2}, \tag{64}$$

and a-index recurrence

$$I^1_{2a,0} = \frac{2a-1}{2a}\, I^1_{2a-2,0}, \qquad I^0_{2a,0} = \frac{(2a-2)\left(1+k_j^2\right)\, I^0_{2a-2,0} - (2a-3) I^0_{2a-4,0}}{(2a-1)k_j^2}, \tag{65}$$

we may continue using (61) and (63) to obtain any required $I^c_{2a,2b}$. As a matter of fact, the case of $I^1_{2a,0}$ can be handled directly because (64) and (65) imply

$$I^1_{2a,0} = (-1)^a P_{2a}(0). \tag{66}$$

Although it occurred that all results of the present work are expressible in terms of $I^1_{2a,2b}$, we retain $I^0_{2a,2b}$ rules for completeness.

4.4.2 Variables G and Δ

Let us switch back from $\boldsymbol{w}_{n,m}$ to the basic $\boldsymbol{v}_{n,m}$ vectors and introduce the following symbols:

$$x_{n,m} = \Re(\boldsymbol{v}_{n,m}) \cdot \hat{\boldsymbol{b}}_1, \qquad y_{n,m} = \Im(\boldsymbol{v}_{n,m}) \cdot \hat{\boldsymbol{b}}_2, \qquad z_{n,m} = \Re(\boldsymbol{v}_{n,m}) \cdot \hat{\boldsymbol{b}}_3, \tag{67}$$

using the real and imaginary part operators $\Re$, $\Im$ and

$$X^{n,m}_{q,j} = (-1)^{\lfloor (q+1)/2 \rfloor} \binom{m}{q} \frac{c_{n,m,j}\, P_n(0)}{n(n+1)}\, S_1^{m-q} S_2^q S_3^{n-m-2j}. \tag{68}$$

Elementary manipulations lead to the final results for the SAM

$$\left\langle \dot{G} \right\rangle_{\rm S} = -\frac{\kappa}{\eta_{\rm s}} \frac{\pi}{2K_3} \sum_{n\geq 1} \Theta_{2n}(\cos\varepsilon)\, G_{3,n}, \tag{69}$$

$$G_{3,n} = \frac{z_{2n,0}\, C_{n,0}}{2} + \sum_{m=1}^{n} \left(x_{2n,2m-1} A_{n,m} + y_{2n,2m-1} B_{n,m} + z_{2n,2m}\, C_{n,m} \right), \tag{70}$$

$$A_{n,m} = \frac{4n(2n+1)}{\sigma_{2n,0}} S_1 \sum_{q=0}^{m-1} \sum_{j=0}^{n-m} X^{2n,2m-1}_{2q,j}\, I^{2(n-m-j)+1}_{2q,2(m-q)}, \tag{71}$$

$$B_{n,m} = \frac{4n(2n+1)}{\sigma_{2n,0}} S_2 \sum_{q=0}^{m-1} \sum_{j=0}^{n-m} X^{2n,2m-1}_{2q+1,j}\, I^{2(n-m-j)+1}_{2(q+1),2(m-q-1)}, \tag{72}$$

$$C_{n,m} = \frac{4n(2n+1)}{\sigma_{2n,0}} S_3 \sum_{q=0}^{m} \sum_{j=0}^{n-m} X^{2n,2m}_{2q,j}\, I^{2(n-m-j)+1}_{2q,2(m-q)}, \tag{73}$$

where normalized Legendre polynomials $\Theta_n(x) = \sigma_{n,0} P_n(x)$ are introduced.

In the LAM, using

$$Z^{n,m}_{q,j} = (-1)^{\lfloor (q+1)/2 \rfloor} \binom{m}{q} \frac{c_{n,m,j}\, P_n(0)}{n(n+1)}\, L_1^{m-q} L_2^q L_3^{n-m-2j}, \tag{74}$$

we obtain

$$\left\langle \dot{G} \right\rangle_{\rm L} = -\frac{\kappa}{\eta_{\rm s}} \frac{\pi}{2K_1} \sum_{n\geq 1} \Theta_{2n}(\cos\varepsilon)\, G_{1,n}, \tag{75}$$

$$G_{1,n} = \frac{x_{2n,0}\, A'_{n,0}}{2} + \sum_{m=1}^{n} \left(x_{2n,2m} A'_{n,m} + y_{2n,2m} B'_{n,m} + z_{2n,2m-1}\, C'_{n,m} \right), \tag{76}$$

$$A'_{n,m} = \frac{4n(2n+1)}{\sigma_{2n,0}} L_1 \sum_{q=0}^{m} \sum_{j=0}^{n-m} Z^{2n,2m}_{2q,j}\, I^{2(m-q)+1}_{2q,2(n-m-j)}, \tag{77}$$

$$B'_{n,m} = \frac{4n(2n+1)}{\sigma_{2n,0}} L_2 \sum_{q=0}^{m-1} \sum_{j=0}^{n-m} Z^{2n,2m}_{2q+1,j}\, I^{2(m-q)-1}_{2(q+1),2(n-m-j)}, \tag{78}$$

$$C'_{n,m} = \frac{4n(2n+1)}{\sigma_{2n,0}} L_3 \sum_{q=0}^{m-1} \sum_{j=0}^{n-m} Z^{2n,2m-1}_{2q,j}\, I^{2(m-q)-1}_{2q,2(n-m-j+1)}. \tag{79}$$

According to relation (57), the averaged equation for Δ is similar to that of G. Introducing

$$q_j = 1 - a_j \Delta, \tag{80}$$

we have

$$\left\langle \dot{\Delta} \right\rangle_{\rm S} = -\frac{\kappa\,\Delta}{G\,\eta_{\rm s}}\frac{\pi}{K_3}\sum_{n\geq 1}\Theta_{2n}(\cos\varepsilon)\,\Delta_{3,n} \tag{81}$$

$$\Delta_{3,n} = \frac{q_3\,z_{2n,0}\,C_{n,0}}{2} + \sum_{m=1}^{n}\left(q_1\,x_{2n,2m-1}\,A_{n,m} + q_2\,y_{2n,2m-1}\,B_{n,m} + q_3\,z_{2n,2m}\,C_{n,m}\right), \tag{82}$$

and

$$\left\langle \dot{\Delta} \right\rangle_{\rm L} = -\frac{\kappa\,\Delta}{G\,\eta_{\rm s}}\frac{\pi}{K_1}\sum_{n\geq 1}\Theta_{2n}(\cos\varepsilon)\,\Delta_{1,n}, \tag{83}$$

$$\Delta_{1,n} = \frac{q_1\,x_{2n,0}\,A'_{n,0}}{2} + \sum_{m=1}^{n}\left(q_1\,x_{2n,2m}A'_{n,m} + q_2\,y_{2n,2m}B'_{n,m} + q_3\,z_{2n,2m-1}\,C'_{n,m}\right). \tag{84}$$

All Symbols $G_{j,n}$ and $\Delta_{j,n}$ designate functions of dynamical inertia Δ and body specific parameters: moments of inertia and shape coefficients. Their explicit expressions up to $n = 2$ are given in Appendix C.

4.4.3 Obliquity ε

Although equation (56) looks simple, the direct substitution of equations (51) and (52) and

$$\hat{\boldsymbol{j}} = \cos l\,\hat{\boldsymbol{b}}_1 - \sin l\,\hat{\boldsymbol{b}}_2, \qquad \hat{\boldsymbol{t}}_3 \times \hat{\boldsymbol{j}} = \cos J\sin l\,\hat{\boldsymbol{b}}_1 + \cos J\cos l\,\hat{\boldsymbol{b}}_2 - \sin J\,\hat{\boldsymbol{b}}_3 \tag{85}$$

introduces negative powers of $\sin J$ and $\cos J$. Yet, the application of a recurrence formula

$$\sin J\,\sigma^{+}_{n,m}\,{\rm e}^{-{\rm i}l}Y_{n,m-1}\left(\hat{\boldsymbol{t}}_3|\,\mathcal{B}\right) - \sin J\,\sigma^{-}_{n,m}\,{\rm e}^{{\rm i}l}Y_{n,m+1}\left(\hat{\boldsymbol{t}}_3|\,\mathcal{B}\right) = 2{\rm i}\,m\cos J\,Y_{n,m}\left(\hat{\boldsymbol{t}}_3|\,\mathcal{B}\right) \tag{86}$$

helps to achieve the non-singular form

$$\langle\dot{\varepsilon}\rangle_{\rm op} = -\frac{\kappa}{G}\sum_{n\geq 1}\frac{\Theta^1_{2n}(\cos\varepsilon)}{2\,\sigma_{2n,-1}}\sum_{m=-2n}^{2n}\sum_{j=1}^{3}Q^{j}_{2n,m}\,\boldsymbol{w}_{2n,m}\cdot\hat{\boldsymbol{b}}_j, \tag{87}$$

$$Q^1_{2n,m} = \left(\sigma^{-}_{2n,m}\,Y_{2n,m+1}\left(\hat{\boldsymbol{t}}_3|\,\mathcal{B}\right) - \sigma^{+}_{2n,m}\,Y_{2n,m-1}\left(\hat{\boldsymbol{t}}_3|\,\mathcal{B}\right)\right)(\hat{\boldsymbol{t}}_3\cdot\hat{\boldsymbol{b}}_3) - 2\,{\rm i}\,m\,(\hat{\boldsymbol{t}}_3\cdot\hat{\boldsymbol{b}}_2)\,Y_{2n,m}\left(\hat{\boldsymbol{t}}_3|\,\mathcal{B}\right), \tag{88}$$

$$Q^2_{2n,m} = -{\rm i}\,\left(\sigma^{-}_{2n,m}\,Y_{2n,m+1}\left(\hat{\boldsymbol{t}}_3|\,\mathcal{B}\right) + \sigma^{+}_{2n,m}\,Y_{2n,m-1}\left(\hat{\boldsymbol{t}}_3|\,\mathcal{B}\right)\right)(\hat{\boldsymbol{t}}_3\cdot\hat{\boldsymbol{b}}_3) + 2\,{\rm i}\,m\,(\hat{\boldsymbol{t}}_3\cdot\hat{\boldsymbol{b}}_1)\,Y_{2n,m}\left(\hat{\boldsymbol{t}}_3|\,\mathcal{B}\right), \tag{89}$$

$$Q^3_{2n,m} = -\sigma^{-}_{2n,m}\,(\hat{\boldsymbol{t}}_3\cdot\hat{\boldsymbol{b}}_1 - {\rm i}\,\hat{\boldsymbol{t}}_3\cdot\hat{\boldsymbol{b}}_2)\,Y_{2n,m+1}\left(\hat{\boldsymbol{t}}_3|\,\mathcal{B}\right) + \sigma^{+}_{2n,m}\,(\hat{\boldsymbol{t}}_3\cdot\hat{\boldsymbol{b}}_1 + {\rm i}\,\hat{\boldsymbol{t}}_3\cdot\hat{\boldsymbol{b}}_2)\,Y_{2n,m-1}\left(\hat{\boldsymbol{t}}_3|\,\mathcal{B}\right). \tag{90}$$

Then the complete average of the $\dot{\varepsilon}$ in the SAM case is

$$\langle\dot{\varepsilon}\rangle_{\rm S} = -\frac{\kappa}{G\,\eta_{\rm s}}\,\frac{\pi}{2K_3}\sum_{n\geq 1}\Theta^1_{2n}(\cos\varepsilon)\,E_{3,n}, \tag{91}$$

$$E_{3,n} = z_{2n,0}H_n + \sum_{m=1}^{n}\left(x_{2n,2m-1}F_{n,m} + y_{2n,2m-1}G_{n,m} + z_{2n,2m}\,H_{n,m}\right), \tag{92}$$

$$H_n = \frac{1}{\sigma_{2n,1}}\sum_{j=0}^{n-1}(2n-2j)\,X^{2n,0}_{0,j}\,S_3^{-1}\left(S_1^2 I^{2n-2j-1}_{0,2} + S_2^2 I^{2n-2j-1}_{2,0}\right), \tag{93}$$

$$F_{n,m} = \frac{1}{\sigma_{2n,1}}\sum_{q=0}^{m}\sum_{j=0}^{n-m+1}(2-4m)X^{2n,2m-1}_{2q-1,j}\,S_2\,I^{2(n-m-j)+1}_{2q,2(m-q)} + S_3\left(\sigma^{-}_{2n,2m-1}X^{2n,2m}_{2q,j}\,I^{2(n-m-j)+1}_{2q,2(m-q)} - \sigma^{+}_{2n,2m-1}X^{2n,2m-2}_{2q,j}\,I^{2(n-m-j)+3}_{2q,2(m-q-1)}\right), \tag{94}$$

$$G_{n,m} = \frac{1}{\sigma_{2n,1}}\sum_{q=0}^{m}\sum_{j=0}^{n-m+1}(2-4m)X^{2n,2m-1}_{2q,j}\,S_1\,I^{2(n-m-j)+1}_{2q,2(m-q)} + S_3\left(\sigma^{-}_{2n,2m-1}X^{2n,2m}_{2q,j}\,I^{2(n-m-j)+1}_{2q,2(m-q)} + \sigma^{+}_{2n,2m-1}X^{2n,2m-2}_{2q,j}\,I^{2(n-m-j)+3}_{2q,2(m-q-1)}\right), \tag{95}$$

$$\begin{aligned} H_{n,m} = {} & \frac{1}{\sigma_{2n,1}}\sum_{q=0}^{m}\sum_{j=0}^{n-m}S_2\left(\sigma^{+}_{2n,2m}X^{2n,2m-1}_{2q+1,j}\,I^{2(n-m-j)+1}_{2(q+1),2(m-q-1)} + \sigma^{-}_{2n,2m}X^{2n,2m+1}_{2q+1,j}\,I^{2(n-m-j)-1}_{2(q+1),2(m-q)}\right) \\ & + S_1\left(\sigma^{+}_{2n,2m}X^{2n,2m-1}_{2q,j}\,I^{2(n-m-j)+1}_{2q,2(m-q)} - \sigma^{-}_{2n,2m}X^{2n,2m+1}_{2q,j}\,I^{2(n-m-j)-1}_{2q,2(m-q+1)}\right), \end{aligned} \tag{96}$$

and its LAM counterpart reads

$$\langle\dot{\varepsilon}\rangle_{\rm L} = -\frac{\kappa}{G\,\eta_{\rm s}}\,\frac{\pi}{2K_1}\sum_{n\geq 1}\Theta^1_{2n}(\cos\varepsilon)\,E_{1,n}, \tag{97}$$

$$E_{1,n} = x_{2n,0} F'_n + \sum_{m=1}^{n} \left(x_{2n,2m} F'_{n,m} + y_{2n,2m} G'_{n,m} + z_{2n,2m-1}\, H'_{n,m} \right), \tag{98}$$

$$F'_n = \frac{\sqrt{2n(2n+1)}}{\sigma_{2n,1}} L_3 \sum_{j=0}^{n-1} Z_{0,j}^{2n,1}\, I_{0,2(n-j)}^{1}, \tag{99}$$

$$F'_{n,m} = \frac{1}{\sigma_{2n,1}} \sum_{q=0}^{m} \sum_{j=0}^{n-m} (-4m)\, L_2 Z_{2q+1,j}^{2n,2m}\, I_{2q+2,2(n-m-j)}^{2(m-q)-1} + L_3 \left(\sigma_{2n,2m}^{-} Z_{2q,j}^{2n,2m+1}\, I_{2q,2(n-m-j)}^{2(m-q)+1} - \sigma_{2n,2m}^{+} Z_{2q,j}^{2n,2m-1}\, I_{2q,2(n-m-j+1)}^{2(m-q)-1} \right), \tag{100}$$

$$G'_{n,m} = \frac{1}{\sigma_{2n,1}} \sum_{q=0}^{m} \sum_{j=0}^{n-m} (-4m)\, L_1 Z_{2q,j}^{2n,2m}\, I_{2q,2(n-m-j)}^{2(m-q)+1} + L_3 \left(\sigma_{2n,2m}^{-} Z_{2q,j}^{2n,2m+1}\, I_{2q,2(n-m-j)}^{2(m-q)+1} + \sigma_{2n,2m}^{+} Z_{2q,j}^{2n,2m-1}\, I_{2q,2(n-m-j+1)}^{2(m-q)-1} \right), \tag{101}$$

$$\begin{aligned} H'_{n,m} = {} & \frac{1}{\sigma_{2n,1}} \sum_{q=0}^{m} \sum_{j=0}^{n-m+1} L_2 \left(\sigma_{2n,2m-1}^{+} Z_{2q+1,j}^{2n,2m-2}\, I_{2q+2,2(n-m-j+1)}^{2(m-q)-3} + \sigma_{2n,2m-1}^{-} Z_{2q+1,j}^{2n,2m}\, I_{2q+2,2(n-m-j)}^{2(m-q)-1} \right) \\ & + L_1 \left(\sigma_{2n,2m-1}^{+} Z_{2q,j}^{2n,2m-2}\, I_{2q,2(n-m-j+1)}^{2(m-q)-1} - \sigma_{2n,2m-1}^{-} Z_{2q,j}^{2n,2m}\, I_{2q,2(n-m-j)}^{2(m-q)+1} \right). \end{aligned} \tag{102}$$

5 MEAN VARIABLES EVOLUTION

In this section, unless explicitly stated, symbols G_j, Δ_j and ε_j refer to the mean variables, whose evolution is governed by equations (69), (81) and (91) for $j = 3$ (SAM), or (75), (83) and (97) for $j = 1$ (LAM). Discussing first integrals and equilibria, we will also use

$$\xi_j = \cos \varepsilon_j, \qquad \mathcal{A}_j = \frac{1}{\Delta_j}, \tag{103}$$

instead of obliquity and dynamical inertia.

5.1 Quadrupole approximation

Truncating equations of motion at the second degree of insolation series ($n = 1$), we obtain the quadrupole approximation. In this case our results should be equivalent to those of Cicaló & Scheeres (2010), and indeed they are. Truncated equations of motion can be converted to a symmetric form

$$\frac{\mathrm{d}\Delta_j}{-\frac{\kappa\,\Delta_j}{G_j\,\eta_\mathrm{s}}\frac{\pi}{K_j}\,\Theta_2(\xi_j)\,\Delta_{j,1}(\mathcal{A}_j)} = \frac{\mathrm{d}\varepsilon_j}{-\frac{\kappa}{G_j\,\eta_\mathrm{s}}\frac{\pi}{2K_j}\Theta_2^1(\xi_j)\,E_{j,1}(\mathcal{A}_j)} = \frac{\mathrm{d}G_j}{-\frac{\kappa}{\eta_\mathrm{s}}\frac{\pi}{K_j}\,\Theta_2(\xi_j)\,G_{j,1}(\mathcal{A}_j)} = \frac{\mathrm{d}t}{1}. \tag{104}$$

Dropping the last member, we can rewrite this system as

$$\frac{\mathrm{d}\mathcal{A}_j}{-2\mathcal{A}_j\,\frac{\Delta_{j,1}(\mathcal{A}_j)}{G_{j,1}(\mathcal{A}_j)}} = \frac{\mathrm{d}\xi_j}{2\frac{\xi_j-\xi_j^3}{1-3\xi_j^2}} = \frac{\mathrm{d}G_j}{G_j}. \tag{105}$$

The complete separability of (105) is a consequence of two phenomena – both specific for the quadrupole approximation. First, the denominators of $\mathrm{d}\mathcal{A}_j$ and $\mathrm{d}G_j$ contained only a single term which permitted us to cancel $\Theta_2(\xi_j)$. Secondly, for convex bodies with zero conductivity (or within a pseudo-convex approximation) the ratio $E_{j,1}/G_{j,1}$ is a constant number (see Appendix C).

The second equality of (105) generates a first integral

$$\Phi_j(\xi_j, G_j) = \frac{\xi_j\,(1-\xi_j^2)}{G_j^2} = C = \text{const}. \tag{106}$$

This formula alone excludes the possibility of unlimited angular momentum growth for convex/pseudo-convex objects when the quadrupole approximation is used.

Another first integral can be searched either as a function of dynamical inertia and obliquity, as proposed by Cicaló & Scheeres (2010), or as a function of G_j and $\mathcal{A}_j$. The latter choice leads to a simple expression

$$\Psi_j(\mathcal{A}_j, G_j) = G_j^4 \left(\mathcal{A}_j - a_j\right) \left(\mathcal{A}_j - a_j - \beta_j(a_2 - a_j)\right) = C' = \text{const}, \tag{107}$$

where the coefficients β_j depend on the body shape

$$\beta_3 = \frac{8(a_1 - a_3) z_{2,0}}{\sqrt{6}(a_1 - a_2)(z_{2,2} - 2x_{2,1}) + (7a_1 + 3a_2 - 10a_3) z_{2,0}}, \tag{108}$$

$$\beta_1 = \frac{4(a_1 - a_3)(y_{2,2} + z_{2,1})}{2(a_2 - a_3)x_{2,2} + (5a_1 - 3a_2 - 2a_3) y_{2,2} + 5(a_1 - a_2) z_{2,1}}. \tag{109}$$

For typical convex objects the values of β_j are close to 1.

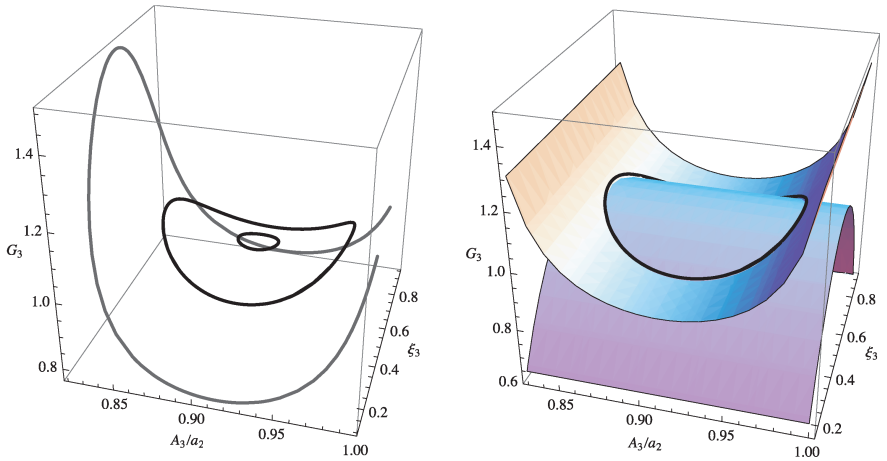

Figure 1. Quadrupole approximation of the YORP perturbed rotation. Left: typical periodic orbits (black) in the $(\mathcal{A}_3, \xi_3, G_3)$ space and an open curve (grey) reaching the boundary $\mathcal{A}_3 = a_2$ in finite time. Right: one of the periodic orbits as an intersection of integral surfaces (106) and (107).

Given two first integrals, the motion in the space of $(\mathcal{A}_j, \xi_j, G_j)$ is confined to the spatial curve being the intersection of two surfaces constructed by sliding the flat curve $\Phi_j = C$ along the $\mathcal{A}_j$ axis and $\Psi_j = C'$ along the ξ_j axis. An example is shown in Fig. 1.

Qualitative features of integral curves on the $(\mathcal{A}_j, \xi_i)$ plane are determined by the location of roots and extremum of the parabola (107). The null-cline of $\dot{\Delta}_j$ is the line of $\mathcal{A}_j$ equal to

$$\mathcal{A}_j^{\rm c} = a_j + \frac{a_2 - a_j}{2}\,\beta_j, \tag{110}$$

where $G_j(\mathcal{A}_j)$ attains the minimum for some specified C'. This value, when combined with the maximum of $G_j(\xi_j)$, defined by

$$\xi_j^{\rm c} = \pm\frac{1}{\sqrt{3}}, \tag{111}$$

i.e. $\varepsilon \approx 55^\circ$, or $\varepsilon \approx 125^\circ$, defines a stable equilibrium (centre type) where, regardless of the value of G_j, all three variables are constant. Close to this equilibrium, the motion can be represented as a closed spatial curve bounded in all three dimensions of $(\mathcal{A}_j, \xi_j, G_j)$ space.

However, the presence of $\mathcal{A}_j^{\rm c}$ in the appropriate interval, i.e. $a_3 < \mathcal{A}_3^{\rm c} < a_2$ or $a_2 < \mathcal{A}_1^{\rm c} < a_1$ depends on particular body shape, requiring $0 < \beta_j < 2$. Additionally, the value $\beta_j = 1$ separates phase portraits with the second root of (107) inside and outside the SAM or LAM bounds. For example, Fig. 1 has been drawn for $\beta_3 \approx 1.05$, so inverting Ψ_3 we have

$$G_3 = \left(\frac{C'}{(\mathcal{A}_3 - a_3)\,(\mathcal{A}_3 - a_3 - \beta_3(a_2 - a_3))}\right)^{\frac{1}{4}}, \tag{112}$$

with one singularity at $\mathcal{A}_3 = a_3$ and one minimum at $a_3 < \mathcal{A}_3^{\rm c} < a_2$, whereas the second singularity is outside the range $(\mathcal{A}_3 = a_3 + \beta_3(a_2 - a_3) > a_2)$. Collection of possible sets of integral curves projected on $(\mathcal{A}_j, \xi_j)$ planes is given in Fig. 2. The same set of plots can be used for SAM $(j = 3)$ and LAM $(j = 1)$, although in the latter case the direction of the horizontal axis should be reversed, because then $a_1 > a_2$.

Generally, our quadrupole truncation is equivalent to the solution of Cicaló & Scheeres (2010), although their figs 8 and 9 do not cover the $1 < \beta_j < 2$ case. Nevertheless, the quadrupole truncation of YORP in mean variables behaves almost like a conservative system. Solutions are either trapped in permanent libration around a stable equilibrium, or they approach the limit of rotation around the intermediate moment of the inertia axis $(\mathcal{A}_j = a_2)$, where the averaging procedure of Section. 4.4 is not valid.

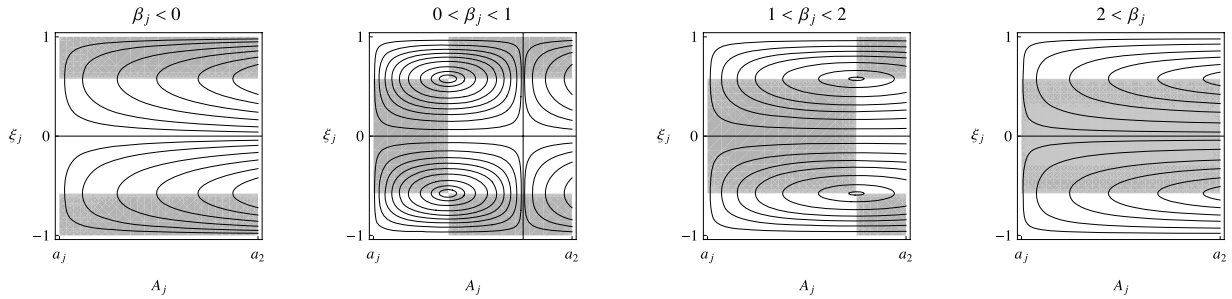

Figure 2. Integral curves of quadrupole approximation projected on the $(\mathcal{A}_j, \xi_j)$ planes. Grey and white areas distinguish the sign of $\dot{G}_j$.

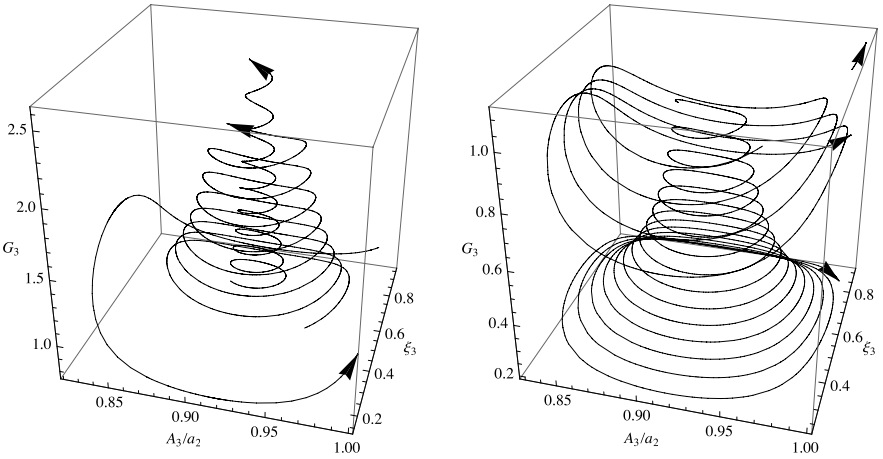

Figure 3. Three orbits with the same initial conditions as in Fig. 1 propagated according to the averaged equations of motion up to $n = 5$. Left: Eger in SAM with $\sigma_3 = 1$. Right: Eger in SAM with $\sigma_3 = -1$.

5.2 General case

First idea about the fundamental difference between the quadrupole approximation and a more complete model can be gained by comparing Fig. 1 with Fig. 3. The latter presents solutions of the averaged system up to degree 10 obtained for the shape of (3103) Eger (see Appendix D) with the same initial conditions as the three curves in Fig. 1. Two panels in Fig. 3 are necessary because, in contrast to the $n = 1$ case, it does matter if the initial SAM state is $\sigma_3 = 1$ or $\sigma_3 = -1$. Two closed cycles from Fig. 1 are replaced by helicoidal curves, because the centre type equilibria on the $(\mathcal{A}_j, \xi_j)$ plane become foci, and they are no longer the fixed points for G_j. As a consequence, two out of the three solutions with $\sigma_3 = 1$ are trapped in this SAM, whereas all three curves with $\sigma_3 = -1$ exit this mode.

If we discuss the complete equations of motion up to any value of n, the equivalent of equation (105) is

$$\frac{\mathrm{d}\mathcal{A}_j}{\mathcal{P}(\mathcal{A}_j, \xi_j)} = \frac{\mathrm{d}\xi_j}{\mathcal{Q}(\mathcal{A}_j, \xi_j)} = \frac{\mathrm{d}G_j}{G_j}, \tag{113}$$

where

$$\mathcal{P}(\mathcal{A}_j, \xi_j) = -2\mathcal{A}_j \frac{\sum_{n\geq 1} \Theta_{2n}(\xi_j)\Delta_{j,n}(\mathcal{A}_j)}{\sum_{n\geq 1} \Theta_{2n}(\xi_j)G_{j,n}(\mathcal{A}_j)}, \tag{114}$$

$$\mathcal{Q}(\mathcal{A}_j, \xi_j) = -\sqrt{1-\xi_j^2}\, \frac{\sum_{n\geq 1} \Theta^1_{2n}(\xi_j)E_{j,n}(\mathcal{A}_j)}{\sum_{n\geq 1} \Theta_{2n}(\xi_j)G_{j,n}(\mathcal{A}_j)}. \tag{115}$$

Equations (113) are only partially separable. First integrals $\Phi_j(\xi_j, G_j)$ and $\Psi_j(\mathcal{A}_j, G_j)$ from Section 5.1 are destroyed when adding terms with $n > 1$. In principle, one may study the Pfaffian equation on a plane

$$\mathcal{Q}(\mathcal{A}_j, \xi_j)\,\mathrm{d}\mathcal{A}_j - \mathcal{P}(\mathcal{A}_j, \xi_j)\,\mathrm{d}\xi_j = 0, \tag{116}$$

independent of G_j, but if the value of G_j systematically decreases, it may reach the limit when either rotation or precession/nutation frequencies become comparable with orbital mean motion and this violates the assumptions of averaging.

An in-depth analysis of equations (113) is beyond the scope of this paper. We are merely going to illustrate how the addition of $n = 2$ (or higher degree terms) affects the conclusions about the evolutionary path of a tumbling object under the action of the YORP torque. Using the torque coefficients from Table D1, we have plotted few generic trajectories on the $(\mathcal{A}_j, \xi_j)$ plane for two SAMs (SP with $\sigma_3 = 1$ and SM[2] with $\sigma_3 = -1$) and two LAMs (LP with $\sigma_1 = 1$ and LM with $\sigma_1 = -1$). Parameters (108) and (109) for Eger are $\beta_3 \approx 1.053$ and $\beta_1 \approx 0.882$, so Fig. 4 illustrates what happens to the two panels of Fig. 2 when the terms of degree 4 (i.e. with $n = 2$) are added. Higher degrees modify the picture only quantitatively. Moreover, taking the mirror image of Eger (shape reflected with respect to the xz plane), we obtain the same plots, except that SP/LP should be interchanged with SM/LM.

Beyond the quadrupole model, the number of equilibria has not been changed, but their location has moved. In particular, two saddles at $\xi_1 = \pm 1$ were pushed out of the plots, having $\mathcal{A}_1 < a_2$ (Fig. 4: LP and LM). Centres are converted into stable or unstable foci (sinks or source points). The equilibria of $\mathcal{A}_j$ and ξ_j no longer lie at the intersection of white and grey areas, but are now associated with some constant, nonzero $\dot{G}_j$. Another new phenomenon is the appearance of limit cycles: stable (LP) and unstable (LM); what looks like thick lines in Fig. 4 is actually the concentration of orbits asymptotically approaching the limit cycle or receding from it. Interestingly, heteroclinic straight lines $\xi_j = 0$ survive the addition of $n > 1$ terms; this is a consequence of the Legendre function skew symmetry $\Theta^1_{2n}(-\xi_j) = -\Theta^1{}_{2n}(\xi_j)$; hence

[2] Usually they are designated SAM_+ and SAM_-, respectively. Similarly, we use LM for LAM_- and LP for LAM_+.

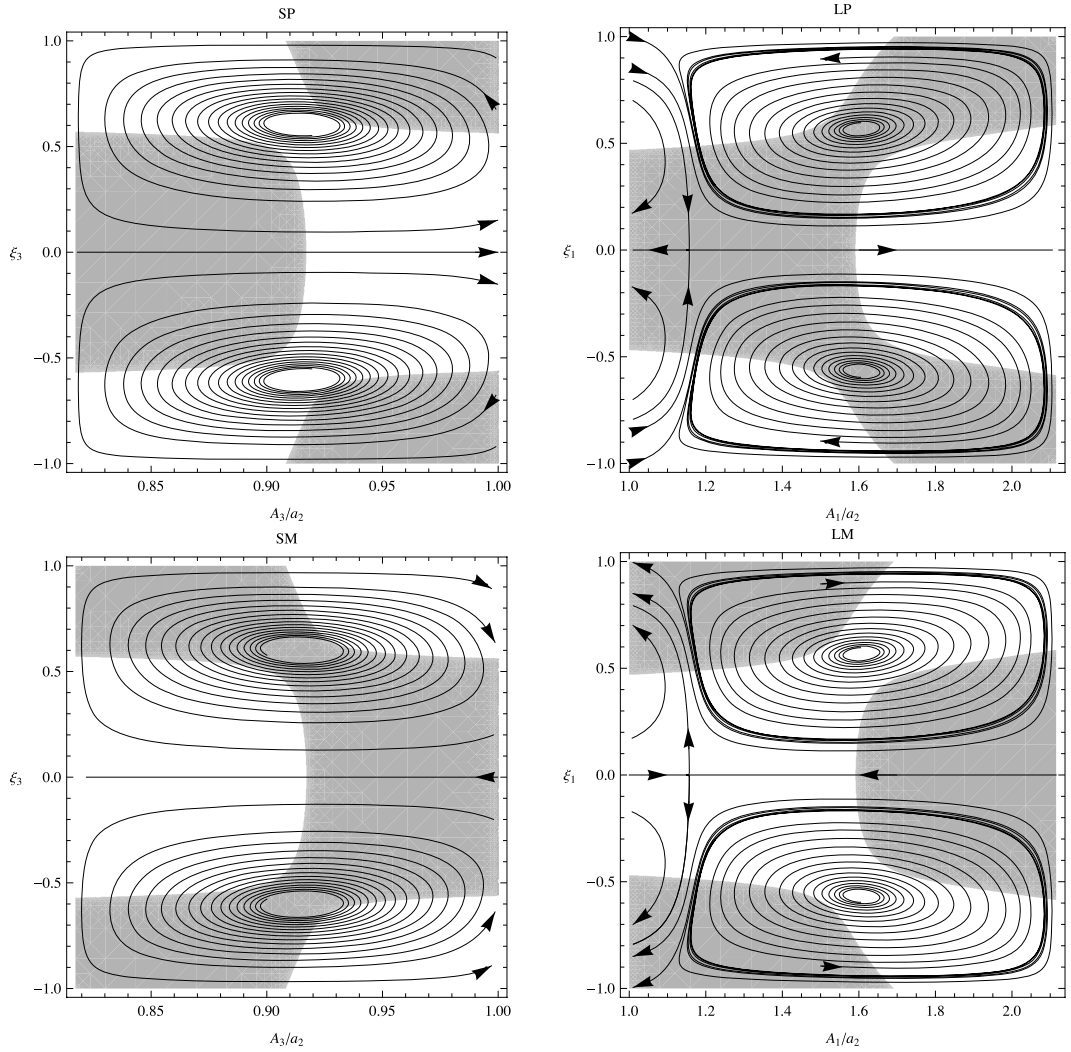

Figure 4. Four possible evolution paths in the 4 degree of approximation for Eger : SAM (left) or LAM (right) with $\sigma_j = 1$ (top) or $\sigma_j = -1$ (bottom). Shaded areas mark $\dot{G}_j < 0$, whereas in white domains G_j increases.

$\Theta^1_{2n}(0) = 0$. The right-hand sides of $\langle \dot{\varepsilon} \rangle$ as well as $\mathcal{P}(\mathcal{A}_j, \xi_j)$ inherit this skew symmetry, so well visible in Fig. 4. Both principal axis modes $\mathcal{A}_j = a_j$ remain unstable solutions regardless of the maximum YORP degree included.

Thinking in terms of the averaged system evolution, we may expect the following evolutionary scenarios for an Eger shaped object.

(i) With initial conditions in SP, the momentum vector either spirals towards the sink ($\mathcal{A}_3 \approx 0.92\, a_2$, $\xi_3 \approx \pm 0.6$) where the momentum G_3 permanently increases or it moves directly to the edge $\mathcal{A}_3 = a_2$. The former case is one of the two final asymptotic states, whereas the latter means leaving the SP mode.

(ii) All trajectories originating in SM approach the edge $\mathcal{A}_3 = a_2$ and exit this mode.

(iii) Most of the solution curves that enter LM or LP through the $\mathcal{A}_1 = a_2$ edge leave these modes quickly, except the $|\xi_1| \approx 1$ in LP which are attracted by a stable limit cycle. The limit cycle also attracts all solution curves that originate inside it.

(iv) If the evolution begins inside the limit cycle of LM, the momentum vector is asymptotically driven towards the sink ($\mathcal{A}_1 \approx 1.6\, a_2$, $\xi_1 \approx \pm 0.6$), where the systematic increase of G_1 stabilizes the final state.

Leaving one of the four modes is a phenomenon related to the original, non-averaged problem. From the point of view of mean variables, the boundary $\mathcal{A}_j = a_2$ cannot be crossed or even reached, being the singular line with an infinite precession period (the assumptions of averaging are violated). Similar to the paradigmatic perturbed pendulum case, a chaotic zone may develop in the vicinity of this boundary, provided the perturbation is strong enough (i.e. for sufficiently small and/or slowly rotating objects).

Overall, unless the motion start inside the stable limit cycle of LM, the most likely outcome of the Eger spin evolution is the capture in SAM with obliquity ε close to 55° or 125° and angle J oscillating between about 15° and 50° (the values implied by $\mathcal{A}_3 \approx 0.92\, a_2$). For the mirror image of Eger, the departure of the momentum vector from the body frame vector $\hat{\boldsymbol{b}}_3$ should oscillate in the range $130^\circ \lesssim J \lesssim 165^\circ$. Using the classification of Vokrouhlický & Čapek (2002), in the principal axis mode (SP, $\mathcal{A}_3 = a_3$) Eger is a Type II object, whereas

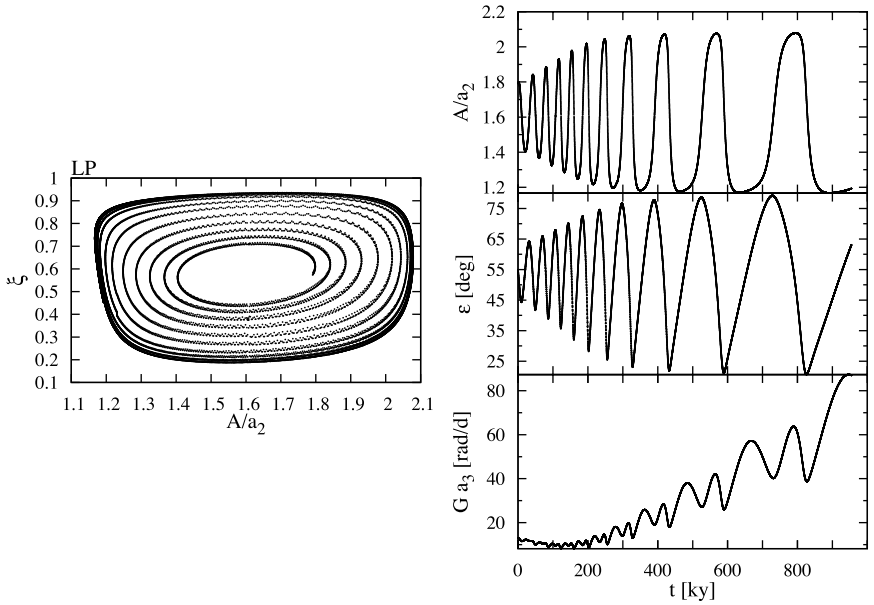

Figure 5. Full solution attracted by the limit cycle. Compare with the LP of Fig. 4.

its mirror image is Type I. We may conjecture that the two asymptotic states should be typical for all convex objects of these YORP types, respectively.

The fate of trajectories attracted to stable limit cycles is not certain. It depends on the net change of momentum per one loop on the $(\mathcal{A}_1, \xi_1)$ plane because the cycle passes through both areas of positive and negative $\dot{G}_1$. If the net effect increases G_1 and the cycle passes sufficiently far from the chaotic zone of $\mathcal{A}_1 \approx a_2$, the limit cycle at LP can be an asymptotic state (as it happens for our Eger and mirrored Eger shapes). But if the momentum systematically decreases, the chaotic zone will grow and finally destroy the limit cycle.

6 NON-AVERAGED DYNAMICS SIMULATION

In order to confront the evolutionary scenarios implied by the perturbation theory in mean variables with the full solution of the YORP torque influence, we performed numerical integration of the system of nine equations for the angular velocity vector $\boldsymbol{\Omega}$, position vector of the Sun $\boldsymbol{r}_\mathrm{s}$ and its conjugate momentum – all three in the body frame. Orbital motion was Keplerian and circular. The only torque acting on an integrated object was the YORP effect $\boldsymbol{M}$ given by equation (29). We used the most reliable numerical integration method: a Taylor series integrator with variable stepsize and order. The code was generated by means of the TIDES 1.2 package[3] created at the University of Zaragoza.

Compared to the method and the model applied by Vokrouhlický et al. (2007), the present software is not only coherent with the departure point of the analytical model (gravitational torques have been removed, the YORP torque approximated by spherical harmonics), but is also beyond suspicion regarding the use of the fixed integration step. We used the model of the same shape that was used in Section 5 – the shape of 3103 Eger. However, in order to speed up the evolution, the size of the object has been scaled down to the 40m effective diameter (diameter of a sphere with the same volume). We performed simulations with three truncation levels of torque $\boldsymbol{M}$ defined in equation (29): up to $Y_{2,2}$ according to the quadrupole model of Section 5.1 or Cicaló & Scheeres (2010) up to $Y_{4,4}$, like in Fig. 4, and up to $Y_{6,6}$.

Roughly speaking, the computations confirmed the existence of the substantial difference between the quadrupole approximation of the YORP effect and the motion under the action of a torque including higher degree terms of the insolation function expansion. On the other hand, the difference between the approximations of degrees 4 and 6 amounts to a quantitative correction. In these circumstances, we present only a small sample of typical evolutionary paths for the scaled Eger with the torque including the vector coefficients $\boldsymbol{v}_{p,m}$ and spherical harmonics $Y_{p,m}$ up to $p = 4$. In all test runs, the radius of the circular orbit was $r_\mathrm{s} = a_\mathrm{s} = 2$ au, the initial rotation rate was set to $\Omega = 30\,\mathrm{rad\,d^{-1}}$ and $h = g = f_\mathrm{s} = 0$.

Fig. 5 confirms the presence of stable limit cycles in the full (i.e. non-averaged) solution. Initial conditions for this simulation were close to the unstable (source) equilibrium of the LAM tumbling (see Fig. 4, panel LP), namely $l = 90^\circ$, $\varepsilon = 55^\circ$, $J = 60^\circ$; hence, $\xi \approx 0.57$ and $\mathcal{A} \approx 1.79\,a_2$. Subsequent dots on the plot are spaced by 50 years. In spite of some noise due to periodic terms, the shape of the limit cycle fairly coincides with the averaged solution. What is most important, the angular momentum G oscillates, but with a systematic trend that speeds up rotation. And since the YORP perturbation strength is inversely proportional to G, the period of limit cycle increases in the plots of $\varepsilon(t)$ and $\mathcal{A}(t)$.

[3] Available at http://gme.unizar.es/software/tides.

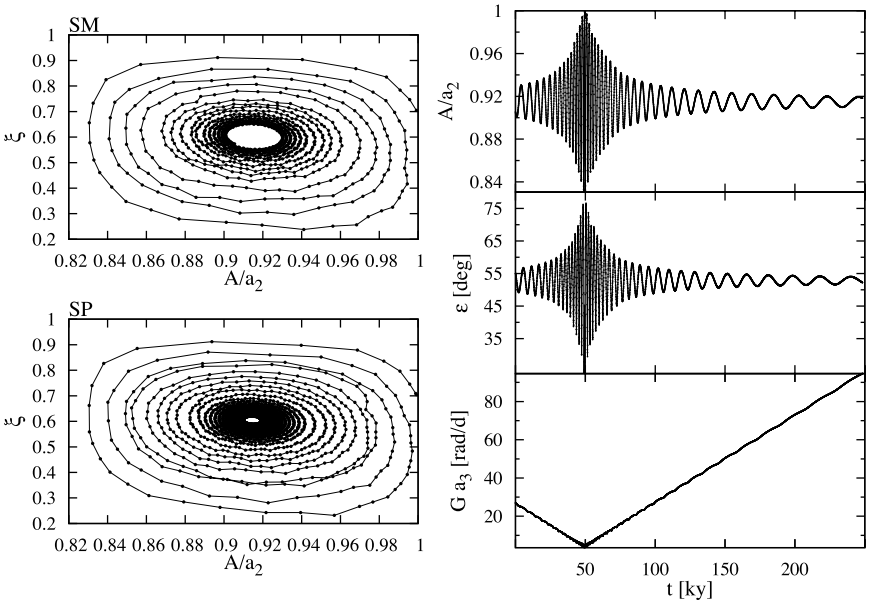

Figure 6. After less than 50 ky the solution leaves the SM region towards the SP asymptotic state. Compare with the SM and SP of Fig. 4.

For the second example we started the integration from $l = 0$, $\varepsilon = 55^\circ$ and $J = 136^\circ$. The evolution presented in Fig. 6 describes a short way from unstable equilibrium (source) of SM to the asymptotically stable sink of SP (see the appropriate panels in Fig. 4). Similar to what was observed in most of the results of Vokrouhlický et al. (2007), rotation tends to the asymptotic state of $\varepsilon \approx 50^\circ$. The magnitude of the angular momentum, initially decreasing, attains the asymptotic state of an unlimited, almost linear growth.

The third example, shown in Fig. 7, describes the fragment of a longer and more varied evolutionary path. The track begins at the point marked A on the composite panel to the left, where the four rotation planes ($\mathcal{A}$, ξ) have been either glued (SAM and LAM) or overlaid (SP with SM and LP with LM). Initial conditions of this point are $l = 270^\circ$, $\varepsilon = 89^\circ$ and $J = 50^\circ$. From the point of view of the secular model (see Fig. 4 LM), the positive value of ξ should remain positive. However, in the non-averaged case the unstable manifold $\xi_1 = 0$ is either deformed or split, allowing the angular momentum vector $\boldsymbol{G}$ to migrate below the orbital plane. Apart from this deviation, the motion follows the path known from Fig. 4 LM, exiting LAM after 250 kyr at the point B, where $\mathcal{A} = a_2$ and $\xi \approx 0.8$. There, the rotation state should jump to another mode, but inspecting the vector fields behind the curves of Fig. 4, we see that jumping to SM or back to LM would involve moving against the current. Out of the two remaining possibilities, the rotation state picks up at SP and continues until mark C, where the next jump is to SM, meaning the evolution back to B. The complete itinerary can be easily deduced from the plots of Fig. 7:

A → B → C → B → C → D → C → D → C → B → E.

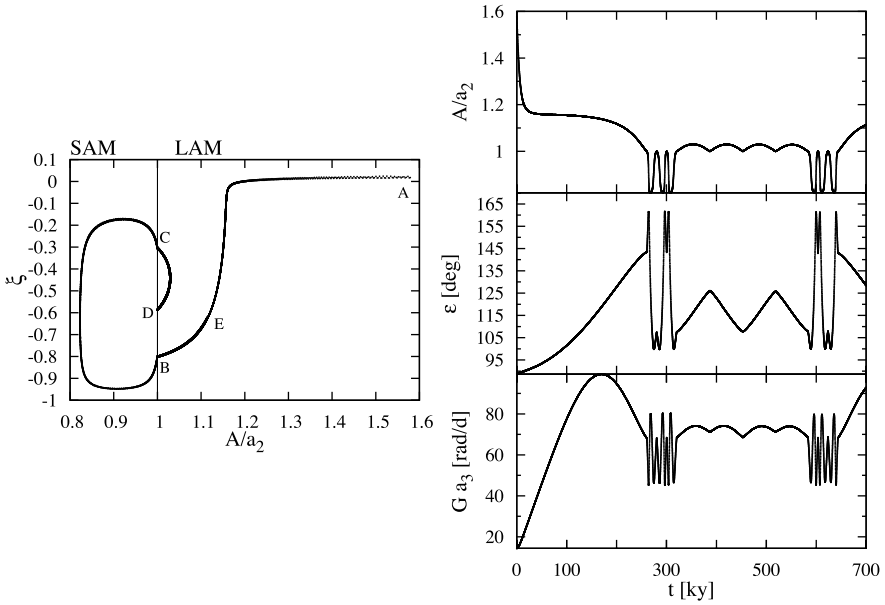

Figure 7. An evolutionary track starting at point A and visiting all four modes from Fig. 4. The simulation was interrupted at E after 700 kyr.

The simulation was interrupted at E, where the subsequent motion is doomed to be trapped by the stable limit cycle of LP, known from Fig. 5.

Interestingly, in all cases the transition between rotation modes is fairly smooth, meaning that the stochastic zone around separatrices is thin – at least for a decametre size object and sufficiently high rotation rates.

7 CONCLUSIONS

Thanks to the use of spherical harmonic series with vectorial coefficients (29), we have constructed a semi-analytical theory (i.e. equations of motion for the secular system) of the Euler–Poinsot problem perturbed by the YORP torque for an object moving on a Keplerian orbit. Although we focused on the application to convex bodies, where the vectorial YORP coefficients are directly related to the Legendre series approximation of the insolation function, the final expressions require only the knowledge of $\boldsymbol{v}_{n,m}$ vectors numerically derivable from any insolation model with an arbitrary scattering/emission law by the application of discrete spherical harmonics transform.

Our theory, valid up to an arbitrary degree and order of YORP harmonics, sheds light on the fundamental difference between the models based upon the second degree harmonics [quadrupole approximation known from Cicaló & Scheeres (2010)] and a more general case. As a matter of fact, the quadrupole approximation behaves like a conservative system and does not allow unbounded solutions for the angular momentum, as far as the first-order perturbations are considered. Starting from degree 4, the unlimited growth of the rotation rate is a generic limit of spin evolution, in agreement with the numerical simulations of Vokrouhlický et al. (2007). Thus, we have resolved the contradiction between the two papers, confirming one of the hints formulated by Cicaló & Scheeres (2010). On the other hand, the present solution validates the integrator described by Vokrouhlický et al. (2007) with its fixed integration step susceptible of introducing an artificial secular trend.

Using an accurate Taylor series integrator we have confirmed that basic conclusions drawn from the secular system remain qualitatively valid in the original problem. Motion under the YORP torque, projected on the plane of obliquity and dynamical inertia, involves not only isolated critical points, but also limit cycles. These of the points and cycles that are asymptotically stable become the 'asymptotic states' [using the terminology of Vokrouhlický et al. (2007)]. Interestingly, only the asymptotic states related to critical points have been detected earlier, whereas those involving limit cycles passed unnoticed. The most likely explanation of this omission is that the initial conditions in Vokrouhlický et al. (2007) were selective. Indeed, all test objects started close to the ($\mathcal{A} \approx a_3, \xi \approx 0.5$) point on the SP panel of Fig. 4 and none of them reached an appropriate basin of the attraction of the limit cycle.

We have used only two test objects (Eger and its mirror image) but, since the present study corroborates the numerical results of Vokrouhlický et al. (2007), the sample of 10 other bodies integrated in that paper can be used as an argument for the significance of higher degree terms in the insolation function for a generic shape.

Obviously, the implications of the YORP-perturbed Euler–Poinsot problem contradict observational facts. Most of all, in the pure YORP problem the principal axis rotation state of asteroids is unstable and unlikely to be observed, whereas the majority of known rotation states are in an almost perfect principal axis mode. Such a disagreement suggests a necessary extension of our present solution by the inclusion of anelastic energy dissipation as the most probable remedy. Such work is now in progress.

ACKNOWLEDGMENTS

The work of SB and AR was supported by the Polish Ministry of Science and Higher Education – grant no. N N203 302535. The work of DV was supported by Czech Grant Agency (grant no. 205/08/0064) and the Research Program MSM0021620860 of the Czech Ministry of Education.

REFERENCES

Biedenharn L. C., Louck J. D., 1981, Angular Momentum in Quantum Physics. Addison-Wesley, Reading
Breiter S., Michalska H., 2008, MNRAS, 388, 927
Breiter S., Vokrouhlický D., 2011, MNRAS, 410, 2807
Breiter S., Bartczak P., Czekaj M., Oczujda B., Vokrouhlický D., 2009, A&A, 507, 1073
Breiter S., Bartczak P., Czekaj M., 2010, MNRAS, 408, 1576
Cicaló S., Scheeres D. J., 2010, Celest. Mech. Dynamical Astron., 106, 301
Deprit A., Elipe A., 1993, J. Astron. Sci., 41, 603
Gurfil P., Elipe A., Tangren W., Efroimsky M., 2007, Regular Chaotic Dynamics, 12, 389
Kaasalainen M., Ďurech J., Warner B. D., Krugly Y. N., Gaftonyuk N. M., 2007, Nat, 446, 420
Kinoshita H., 1972, PASJ, 24, 423
Lowry S. C. et al., 2007, Sci, 316, 272
Mysen E., 2007, MNRAS, 381, 301
Mysen E., 2008, A&A, 484, 563
Nesvorný D., Vokrouhlický D., 2007, AJ, 134, 1750
Nesvorný D., Vokrouhlický D., 2008, AJ, 136, 291
Paddack S. J., 1969, J. Geophys. Res., 74, 4379
Pravec P. et al., 2008, Icarus, 197, 497
Pravec P. et al., 2010, Nat, 466, 1085
Rubincam D. P., 2000, Icarus, 148, 2

Sadov I. A., 1970, Prikladnaya Matematika Mekhanika, 34, 962
Scheeres D. J., Gaskell R. W., 2008, Icarus, 198, 125
Scheeres D. J., Mirrahimi S., 2008, Celest. Mech. Dynamical Astron., 101, 69
Sharma I., Burns J. A., Hui C.-Y., 2005, MNRAS, 359, 79
Statler T. S., 2009, Icarus, 202, 502
Taylor P. A. et al., 2007, Sci, 316, 274
Vokrouhlický D., Čapek D., 2002, Icarus, 159, 449
Vokrouhlický D., Nesvorný D., Bottke W. F., 2003, Nat, 425, 147
Vokrouhlický D., Brož M., Bottke W. F., Nesvorný D., Morbidelli A., 2006, Icarus, 182, 118
Vokrouhlický D., Breiter S., Nesvorný D., Bottke W. F., 2007, Icarus, 191, 636
Walsh K. J., Richardson D. C., Michel P., 2008, Nat, 454, 188
Ďurech et al., 2008, A&A, 489, L25
Ďurech J. et al., 2011, A&A, submitted

APPENDIX A: SPECIAL FUNCTIONS

Given a unit vector $\hat{\boldsymbol{u}}$ in a specified orthonormal basis $\mathcal{E} = (\hat{\boldsymbol{e}}_1, \hat{\boldsymbol{e}}_2, \hat{\boldsymbol{e}}_3)$

$$\hat{\boldsymbol{u}} = \sin\theta\cos\phi\,\hat{\boldsymbol{e}}_1 + \sin\theta\sin\phi\,\hat{\boldsymbol{e}}_2 + \cos\theta\,\hat{\boldsymbol{e}}_3, \tag{A1}$$

we define the normalized spherical harmonic of degree n and order m in this basis:

$$Y_{n,m}(\hat{\boldsymbol{u}}|\mathcal{E}) = \Theta_n^m(\cos\theta)\,\mathrm{e}^{\mathrm{i}m\phi} = \Theta_n^m(\hat{\boldsymbol{u}}\cdot\hat{\boldsymbol{e}}_3)\left(\frac{\hat{\boldsymbol{u}}\cdot\hat{\boldsymbol{e}}_1 + \mathrm{i}\,\hat{\boldsymbol{u}}\cdot\hat{\boldsymbol{e}}_2}{|\hat{\boldsymbol{u}}\cdot\hat{\boldsymbol{e}}_1 + \mathrm{i}\,\hat{\boldsymbol{u}}\cdot\hat{\boldsymbol{e}}_2|}\right)^m, \tag{A2}$$

where the normalized associated Legendre function is

$$\Theta_n^m(x) = \sigma_{n,m} P_n^m(x), \tag{A3}$$

with the normalization factor

$$\sigma_{n,m} = \sqrt{\frac{(2n+1)}{4\pi}\frac{(n-m)!}{(n+m)!}}. \tag{A4}$$

The phase convention in $P_n^m(x)$ is such that

$$\Theta_n^m(x) = (-1)^m\Theta_n^{-m}(x), \qquad Y^*_{n,m}(\hat{\boldsymbol{u}}|\mathcal{E}) = (-1)^m\,Y_{n,-m}(\hat{\boldsymbol{u}}|\mathcal{E}). \tag{A5}$$

For $m \geq 0$ the explicit polynomial form

$$Y_{n,m}(\hat{\boldsymbol{u}}|\mathcal{E}) = (\hat{\boldsymbol{u}}\cdot\hat{\boldsymbol{e}}_1 + \mathrm{i}\,\hat{\boldsymbol{u}}\cdot\hat{\boldsymbol{e}}_2)^m \sum_{j=0}^{\lfloor (n-m)/2\rfloor} c_{n,m,j}\,(\hat{\boldsymbol{u}}\cdot\hat{\boldsymbol{e}}_3)^{n-m-2j}, \tag{A6}$$

where $\lfloor x\rfloor$ is the rounding down operator ('floor' function) and

$$c_{n,m,j} = \frac{\sigma_{n,m}(-1)^{m+j}\,(2n-2j)!}{2^n\,j!\,(n-j)!\,(n-m-2j)!}, \tag{A7}$$

can be used, whereas negative orders are computed according to rule (A5).

Let a basis $\mathcal{E}'$ be related to $\mathcal{E}$ by the rotation defined through 3-1-3 Euler angles (α, β, γ), i.e. for any $j \in \{1, 2, 3\}$,

$$\hat{\boldsymbol{e}}'_j = [\mathbf{R}_3(\gamma)\mathbf{R}_1(\beta)\mathbf{R}_3(\alpha)]^{\mathrm{T}}\,\hat{\boldsymbol{e}}_j = [\mathbf{R}(\alpha,\beta,\gamma)]^{\mathrm{T}}\,\hat{\boldsymbol{e}}_j. \tag{A8}$$

The transpose appears due to the use of passive rotation matrices:

$$\mathbf{R}_1(\beta) = \begin{pmatrix} 1 & 0 & 0 \\ 0 & \cos\beta & \sin\beta \\ 0 & -\sin\beta & \cos\beta \end{pmatrix}, \qquad \mathbf{R}_3(\alpha) = \begin{pmatrix} \cos\alpha & \sin\alpha & 0 \\ -\sin\alpha & \cos\alpha & 0 \\ 0 & 0 & 1 \end{pmatrix}. \tag{A9}$$

With this convention we transform the coordinates of a vector,

$$\boldsymbol{u} = u_1\hat{\boldsymbol{e}}_1 + u_2\hat{\boldsymbol{e}}_2 + u_3\hat{\boldsymbol{e}}_3 = u'_1\hat{\boldsymbol{e}}'_1 + u'_2\hat{\boldsymbol{e}}'_2 + u'_3\hat{\boldsymbol{e}}'_3, \tag{A10}$$

as follows:

$$\begin{pmatrix} u'_1 \\ u'_2 \\ u'_3 \end{pmatrix} = \mathbf{R}(\alpha,\beta,\gamma)\begin{pmatrix} u_1 \\ u_2 \\ u_3 \end{pmatrix}. \tag{A11}$$

Changing the basis we transform spherical harmonics according to the rules

$$Y_{n,m}(\hat{\boldsymbol{u}}|\mathcal{E}') = \sum_{k=-n}^{n} D^n_{k,m}(\alpha,\beta,\gamma)\,Y_{n,k}(\hat{\boldsymbol{u}}|\mathcal{E}), \tag{A12}$$

$$Y_{n,m}(\hat{\boldsymbol{u}}|\mathcal{E}) = \sum_{k=-n}^{n} \left[D^n_{m,k}(\alpha,\beta,\gamma)\right]^* \, Y_{n,k}(\hat{\boldsymbol{u}}|\mathcal{E}'), \tag{A13}$$

involving Wigner D-functions. The definition of the Wigner functions for the 3-1-3 angles used in this paper is

$$D^n_{m,k}(\alpha,\beta,\gamma) = \mathrm{i}^{m-k}\, d^n_{m,k}(\beta)\, \mathrm{e}^{-\mathrm{i}\,(m\alpha + k\,\gamma)}, \tag{A14}$$

where the Wigner d-functions,

$$d^n_{m,k}(\beta) = \sqrt{\frac{(n+k)!(n-k)!}{(n+m)!(n-m)!}}\, [\sin(\beta/2)]^{k-m}\, [\cos(\beta/2)]^{k+m}\, P_n^{(k-m,k+m)}(\cos\beta), \tag{A15}$$

are expressed in terms of the Jacobi polynomials $P_n^{(k-m,k+m)}$. Equation (A14) differs from a more common definition in terms of 3-2-3 Euler angles (e.g. Biedenharn & Louck 1981) by the presence of the i^{m-k} factor. In next sections we will use mainly the special cases where at least one of the subscripts is zero. Then

$$d^n_{k,0}(\beta) = (-1)^k d^n_{0,k}(\beta) = \sqrt{\frac{4\pi}{2n+1}}\, \Theta^k_n(\cos\beta). \tag{A16}$$

For a scalar product of two unit vectors, Legendre polynomials $P_n(\hat{\boldsymbol{u}}_1 \cdot \hat{\boldsymbol{u}}_2)$ admit the addition theorem

$$P_n(\hat{\boldsymbol{u}}_1 \cdot \hat{\boldsymbol{u}}_2) = \frac{4\pi}{2n+1} \sum_{m=-n}^{n} Y^*_{n,m}(\hat{\boldsymbol{u}}_1|\mathcal{E})\, Y_{n,m}(\hat{\boldsymbol{u}}_2|\mathcal{E}). \tag{A17}$$

Note that the left-hand side of equation (A17) is real and invariant with respect to rotations, which means that the complete sum to the right is also invariant: $\mathcal{E}$ can be replaced at will by $\mathcal{E}'$:

$$\sum_{m=-n}^{n} Y^*_{n,m}(\hat{\boldsymbol{u}}_1|\mathcal{E})\, Y_{n,m}(\hat{\boldsymbol{u}}_2|\mathcal{E}) = \sum_{m=-n}^{n} Y^*_{n,m}(\hat{\boldsymbol{u}}_1|\mathcal{E}')\, Y_{n,m}(\hat{\boldsymbol{u}}_2|\mathcal{E}'), \tag{A18}$$

and the arguments $\hat{\boldsymbol{u}}_1$ and $\hat{\boldsymbol{u}}_2$ can be interchanged. If we set the order $m = 0$ on the left-hand side of equation (A12) and divide both sides by $\sigma_{n,0}$, then we obtain

$$P_n(\hat{\boldsymbol{u}} \cdot \hat{\boldsymbol{e}}'_3) = \sqrt{\frac{4\pi}{2n+1}} \sum_{k=-n}^{n} D^n_{k,0}(\alpha,\beta,\gamma)\, Y_{n,k}(\hat{\boldsymbol{u}}|\mathcal{E}). \tag{A19}$$

Interpreting this formula in the context of the addition theorem (A17), we identify

$$D^n_{k,0}(\alpha,\beta,\gamma) = \sqrt{\frac{4\pi}{2n+1}}\, Y^*_{n,k}(\hat{\boldsymbol{e}}'_3|\mathcal{E}). \tag{A20}$$

A similar treatment of equation (A13) leads to

$$D^n_{0,k}(\alpha,\beta,\gamma) = \sqrt{\frac{4\pi}{2n+1}}\, Y_{n,k}(\hat{\boldsymbol{e}}_3|\mathcal{E}'). \tag{A21}$$

APPENDIX B: FREE-TOP SOLUTION IN DEPRIT–ELIPE VARIABLES

The appendix is mainly based upon the work of Deprit & Elipe (1993), although we have modified some intermediate variables' definitions, notation and sign conventions. We have also completed a 'left to the reader' part concerning the LAM.

Let $\mathcal{A} = \Delta^{-1}$. The time evolution of γ and δ is

$$\gamma = G\mathcal{A}\, t + \gamma_0, \tag{B1}$$

$$\delta = -\frac{G^2\mathcal{A}^2}{2}\, t, \tag{B2}$$

whereas all remaining variables (h, H, G, Δ) are constant. We assume that time t is measured from the epoch when $\delta = 0$.

In both rotation modes we will use two quantities

$$\alpha = \frac{a_1 - a_2}{a_1 - \mathcal{A}}, \qquad \alpha_0 = \frac{a_1 - a_2}{a_1 - a_3}, \tag{B3}$$

of which only α depends on the inverse dynamical inertia $\mathcal{A}$.

Legendre elliptic integrals are used in this paper with the following definitions. Elliptic integrals of the first, second and third kinds are, respectively,

$$K(\psi,\, k) = \int_0^{\psi} \frac{\mathrm{d}x}{\sqrt{1 - k^2 \sin^2 x}}, \quad E(\psi,\, k) = \int_0^{\psi} \sqrt{1 - k^2 \sin^2 x}\, \mathrm{d}x, \quad \Pi(\alpha_3,\, \psi,\, k) = \int_0^{\psi} \frac{\mathrm{d}x}{(1 - \alpha_3 \sin^2 x)\sqrt{1 - k^2 \sin^2 x}}, \tag{B4}$$

The associated complete integrals are $K(k) = K(\pi/2,\, k)$, $E(k) = E(\pi/2,\, k)$ and $\Pi(\alpha_3,\, k) = \Pi(\alpha_3,\, \pi/2,\, k)$.

B1 Short-axis mode (SAM)

In this mode $a_3 \le \mathcal{A} < a_2 \le a_1$, and $\boldsymbol{G}$ circulates around $\hat{\boldsymbol{b}}_3$. The sign of L, equal to the sign of $\cos J$, is conserved during the circulation. Introducing

$$\sigma_3 = \mathrm{sgn}(\hat{\boldsymbol{t}}_3 \cdot \hat{\boldsymbol{b}}_3) = \pm 1, \tag{B5}$$

we will distinguish the two possible regimes.

An intermediate variable ψ_3 is defined as the Jacobi amplitude

$$\psi_3 = \mathrm{am}\left(-\frac{2\,n_3}{G^2\mathcal{A}^2}\,\delta, k_3\right) = \mathrm{am}\,(n_3\,t, k_3)\,, \tag{B6}$$

where

$$k_3 = \sqrt{\frac{\alpha-\alpha_0}{1-\alpha_0}}, \qquad n_3 = G\sqrt{(a_1-\mathcal{A})(a_2-a_3)}. \tag{B7}$$

The mean value of $\dot{\psi}_3$ is

$$\left\langle \dot{\psi}_3 \right\rangle = \frac{\pi\,n_3}{2\,K_3} = -\sigma_3 \left\langle \dot{l} \right\rangle, \tag{B8}$$

where

$$K_3 = K(k_3). \tag{B9}$$

The motion of $\boldsymbol{G}$ in the body frame can be expressed as the 2π-periodic Fourier series of the angle

$$\overline{\psi}_3 = \frac{\pi\,n_3}{2\,K_3}\,t = -\frac{\pi\,n_3}{G^2\mathcal{A}^2K_3}\,\delta. \tag{B10}$$

or in terms of the Jacobian elliptic functions of $n_3\,t$. Since $||\boldsymbol{G}|| = ||G\hat{\boldsymbol{t}}_3|| = G$ is constant, we consider only the $\mathcal{T}$ basis vector $\hat{\boldsymbol{t}}_3$:

$$\hat{\boldsymbol{t}}_3 \cdot \hat{\boldsymbol{b}}_1 = \sin J\ \sin l = S_1\ \cos\psi_3 = S_1\,\mathrm{cn}(n_3\,t,\ k_3), \tag{B11}$$

$$\hat{\boldsymbol{t}}_3 \cdot \hat{\boldsymbol{b}}_2 = \sin J\ \cos l = S_2\ \sin\psi_3 = S_2\,\mathrm{sn}(n_3\,t,\ k_3), \tag{B12}$$

$$\hat{\boldsymbol{t}}_3 \cdot \hat{\boldsymbol{b}}_3 = \cos J = S_3\sqrt{1-k_3^2\sin^2\psi_3} = S_3\,\mathrm{dn}(n_3\,t,\ k_3), \tag{B13}$$

where

$$S_1 = \sigma_3\sqrt{\frac{\alpha-\alpha_0}{\alpha}}, \qquad S_2 = \sqrt{\frac{\alpha-\alpha_0}{\alpha\,(1-\alpha_0)}}, \qquad S_3 = \sigma_3\sqrt{\frac{\alpha_0}{\alpha}}, \tag{B14}$$

so that

$$S_1^2 - S_2^2 + S_3^2k_3^2 = 0. \tag{B15}$$

The initial epoch $t = 0$ corresponds to $\boldsymbol{G}\cdot\hat{\boldsymbol{b}}_2 = 0$. Depending on the sign σ_3, it implies the initial value of l:

$$l_0 = \sigma_3\,\frac{\pi}{2}. \tag{B16}$$

The motion of $\boldsymbol{G}$ in the fixed frame $\mathcal{S}$ involves γ. Evaluating quadratures differently than Deprit & Elipe (1993), we find the expression of the angle g in terms of γ and $\psi(\delta, \Delta, G)$:

$$g = g_0 + \gamma + \frac{(\alpha_0-\alpha)\,F(\psi_3,\ k_3) + \alpha\,\Pi(\alpha_3, \psi_3,\ k_3)}{\sqrt{\alpha\,\alpha_0\,(1-\alpha_0)}}, \tag{B17}$$

where

$$\alpha_3 = \frac{\alpha_0}{\alpha_0-1}. \tag{B18}$$

The elliptic integral of the first kind is simply $F(\psi_3, k_3) = n_3\,t$. Thus, the precession angle g can be represented as a sum of a mean angle

$$\overline{g}_3 = g_0 + \gamma + \frac{n_3\,\left[\alpha_0-\alpha+\alpha\,K_3^{-1}\Pi(\alpha_3,\ k_3)\right]\,t}{\sqrt{\alpha\,\alpha_0\,(1-\alpha_0)}}, \tag{B19}$$

and a purely periodic function of $\overline{\psi}_3$.

As long as the ratio $|\dot{\overline{\psi}}_3 : \dot{\overline{g}}_3|$ resulting from equations (B10) and (B19) is an irrational number, the SAM motion of the free top can be represented as the Fourier series of two variables, and the mean values can be evaluated by double integrals with respect to two, formally independent angles $\overline{\psi}_3$ and $\overline{g}_3$ – both circulating in the range from 0 to 2π.

B2 Long-axis mode (LAM)

Strictly speaking, the formulae describing SAM are still valid in LAM, but they involve imaginary arguments and modulus greater than 1 when $a_3 \le a_2 < \mathcal{A} \le a_1$. Performing necessary transformation we obtain the following setup.

Let

$$\sigma_1 = \mathrm{sgn}(\hat{\boldsymbol{t}}_3 \cdot \hat{\boldsymbol{b}}_1) = \pm 1, \tag{B20}$$

distinguish two possible regimes of $\hat{\boldsymbol{t}}_3$ circulation around $\hat{\boldsymbol{b}}_1$.

Using

$$k_1 = k_3^{-1} = \sqrt{\frac{1-\alpha_0}{\alpha-\alpha_0}}, \qquad n_1 = G\sqrt{(a_1-a_2)(\mathcal{A}-a_3)}, \tag{B21}$$

we define an intermediate variable ψ_1 in terms of δ:

$$\psi_1 = \mathrm{am}\left(-\frac{2\,n_1}{G^2\mathcal{A}^2}\,\delta, k_1\right) = \mathrm{am}\,(n_1\,t, k_1)\,, \tag{B22}$$

similar to the SAM case. With $K_1 = K(k_1)$, the mean value of $\dot{\psi}_1$ is

$$\left\langle \dot{\psi}_1 \right\rangle = \frac{\pi\,n_1}{2\,K_1}, \tag{B23}$$

but this time l librates around $\pi/2$ or $3\pi/2$, so $\left\langle \dot{\psi}_1 \right\rangle$ refers to the libration frequency of l and not to the secular part like that in equation (B8).

The motion of $\boldsymbol{G}$ in the body frame is described by

$$\hat{\boldsymbol{t}}_3 \cdot \hat{\boldsymbol{b}}_1 = \sin J\ \sin l = L_1\sqrt{1-k_1^2\sin^2\psi_1} = L_1\,\mathrm{dn}(n_1\,t,\ k_1), \tag{B24}$$

$$\hat{\boldsymbol{t}}_3 \cdot \hat{\boldsymbol{b}}_2 = \sin J\ \cos l = L_2\ \sin\psi_1 = L_2\,\mathrm{sn}(n_1\,t,\ k_1), \tag{B25}$$

$$\hat{\boldsymbol{t}}_3 \cdot \hat{\boldsymbol{b}}_3 = \cos J = L_3\ \cos\psi_1 = L_3\,\mathrm{cn}(n_1\,t,\ k_1), \tag{B26}$$

where

$$L_1 = \sigma_1\sqrt{\frac{\alpha-\alpha_0}{\alpha}}, \qquad L_2 = \sigma_1\,\frac{1}{\sqrt{\alpha}}, \qquad L_3 = \sqrt{\frac{\alpha_0}{\alpha}}; \tag{B27}$$

hence

$$L_1^2\,k_1^2 - L_2^2 + L_3^2 = 0. \tag{B28}$$

Within the present sign convention, the initial epoch $t = 0$ corresponds to $l_0 = \sigma_1\pi/2$ and $\cos J_0 > 0$.

The expression of g is quite similar to (B17):

$$g = g_0 + \gamma + \frac{(\alpha_0-\alpha)\,F(\psi_1,\ k_1) + \alpha\,\Pi(\alpha_1,\ \psi_1,\ k_1)}{\sqrt{\alpha\,\alpha_0\,(\alpha-\alpha_0)}}, \tag{B29}$$

with

$$\alpha_1 = \frac{\alpha_0}{\alpha_0-\alpha}. \tag{B30}$$

Similar to the SAM case, g circulates and can split into the sum of a mean angle

$$\overline{g}_1 = g_0 + \gamma + \frac{n_1\,\left[\alpha_0-\alpha+\alpha\,K_1^{-1}\Pi(\alpha_1,\ k_1)\right]\,t}{\sqrt{\alpha\,\alpha_0\,(\alpha-\alpha_0)}}, \tag{B31}$$

and a purely periodic function of $\overline{\psi}_1 = \left\langle \dot{\psi}_1 \right\rangle\,t$.

APPENDIX C: LEADING TERMS OF THE SOLUTION

Interestingly, there exists a number of relations between vectors $\boldsymbol{v}_{n,m}$ for convex bodies. All of them can be derived by combining the integrands of equation (28) with appropriate multipliers until the sum is reduced to a product of some constant and $\hat{\boldsymbol{b}}_j \cdot (\boldsymbol{r}\times\hat{\boldsymbol{n}})$ that integrates to 0 over a closed surface. We have identified the following relations:

$$\begin{aligned}
0 &= \sqrt{3}\,(x_{2,1}-y_{2,1}) - \sqrt{2}\,z_{2,0},\\
0 &= x_{2,0} - \sqrt{6}\,(x_{2,2}-y_{2,2}-z_{2,1}),\\
\sqrt{5}\,z_{2,0} &= -4\sqrt{5}(x_{4,1}-y_{4,1}) + 8z_{4,0},\\
\sqrt{5}\,(x_{2,0}-\sqrt{6}x_{2,2}) &= -6x_{4,0} + 2\sqrt{10}(2x_{4,2}-y_{4,2}) - 2\sqrt{70}(x_{4,4}-y_{4,4}) - 6\sqrt{5}\,z_{4,1} + 2\sqrt{35}z_{4,3}.
\end{aligned} \tag{C1}$$

Below we list explicit formulae that should be substituted in averaged equations for $\dot{G}$, $\dot{\Delta}$ and $\dot{\varepsilon}$. For the SAM case it means equations (69), (81) and (91), and for LAM – (75), (83) and (97).

C1 Short-axis mode

For the quadruple approximation of the illumination function ($n = 1$) we get

$$G_{3,1} = \frac{S_3}{8}\,\left[\sqrt{6}\,\left(S_1^2-S_2^2\right)\,(2x_{2,1}-z_{2,2}) - \left(4-3S_1^2-7S_2^2\right)\,z_{2,0}\right], \tag{C2}$$

$$E_{3,1} = -\sqrt{\frac{2}{3}}\, G_{3,1}, \tag{C3}$$

$$\Delta_{3,1} = G_{3,1} + \frac{\Delta\, S_3}{8}\, \left[-2\sqrt{6}\, \left(a_1 S_1^2 - a_2 S_2^2\right)\, x_{2,1} - \left(4a_2 S_2^2 - a_3\, \left(4 - 3S_1^2 - 3S_2^2\right)\right)\, z_{2,0} + \sqrt{6}\, a_3\, \left(S_1^2 - S_2^2\right) z_{2,2}\right], \tag{C4}$$

and for terms of degree 4 ($n = 2$),

$$\begin{aligned} G_{3,2} = \frac{3S_3}{512}\, \Big[& 4\sqrt{5}\, S_1^2\, \left(21S_1^2 + 7S_2^2 - 16\right) x_{4,1} - 4\sqrt{5}\, S_2^2\, \left(7S_1^2 + 21S_2^2 - 16\right)\, y_{4,1} \\ & - 12\sqrt{35}\, \left(S_1^2 - S_2^2\right)\, \left(S_1^2 x_{4,3} - S_2^2 y_{4,3}\right) + \left(64 - 160S_1^2 + 105S_1^4 - 160S_2^2 + 70S_1^2 S_2^2 + 105S_2^4\right)\, z_{4,0} \\ & + 6\sqrt{10}\, \left(S_1^2 - S_2^2\right) \left(8 - 7S_1^2 - 7S_2^2\right) z_{4,2} + 3\sqrt{70}\, \left(S_1^2 - S_2^2\right)^2 z_{4,4}\Big], \end{aligned} \tag{C5}$$

$$\begin{aligned} E_{3,2} = & -\frac{2}{\sqrt{5}}\, G_{3,2} + \frac{3S_3}{64}\, \big[\left(-8 + 13S_1^2 + 7S_2^2\right) x_{4,1} + \left(8 - 7S_1^2 - 13S_2^2\right) y_{4,1} \\ & - \frac{4}{\sqrt{5}}\, \left(-4 + 5(S_1^2 + S_2^2)\right) z_{4,0} + 3(S_1^2 - S_2^2)(\sqrt{7}\, (y_{4,3} - x_{4,3}) + 2\sqrt{2}\, z_{4,2})\Big], \end{aligned} \tag{C6}$$

$$\begin{aligned} \Delta_{3,2} = G_{3,2} - \frac{3\Delta S_3}{512}\, \Big[& 4\sqrt{5}\, a_1 S_1^2\, \left(21S_1^2 + 7S_2^2 - 16\right) x_{4,1} - 4\sqrt{5}\, a_2 S_2^2\, \left(7S_1^2 + 21S_2^2 - 16\right)\, y_{4,1} \\ & - 12\sqrt{35}\, \left(S_1^2 - S_2^2\right)\, \left(a_1 S_1^2 x_{4,3} - a_2 S_2^2 y_{4,3}\right) + a_3\, \left(64 - 160S_1^2 + 105S_1^4 - 160S_2^2 + 70S_1^2 S_2^2 + 105S_2^4\right)\, z_{4,0} \\ & + 6\sqrt{10}\, a_3\, \left(S_1^2 - S_2^2\right) \left(8 - 7S_1^2 - 7S_2^2\right) z_{4,2} + 3\sqrt{70}\, a_3\, \left(S_1^2 - S_2^2\right)^2 z_{4,4}\Big]. \end{aligned} \tag{C7}$$

C2 Long-axis mode

For the quadruple approximation of the illumination function ($n = 1$) we get

$$G_{1,1} = \frac{L_1}{8}\, \left[\left(2 - 5L_3^2\right) x_{2,0} + \sqrt{6}\, \left(-2 + 2L_2^2 + 3L_3^2\right) x_{2,2} + 2\sqrt{6}\, \left(L_2^2 - L_3^2\right) y_{2,2}\right], \tag{C8}$$

$$E_{1,1} = -\sqrt{\frac{2}{3}}\, G_{1,1}, \tag{C9}$$

$$\Delta_{1,1} = G_{1,1} + \frac{\Delta\, L_1}{8}\, \left[\left(2a_3 L_3^2 - a_1\, \left(2 - 3L_3^2\right)\right) x_{2,0} - \sqrt{6}\, \left(2a_3 L_3^2 + a_1\, \left(-2 + 2L_2^2 + L_3^2\right)\right)\, x_{2,2} - 2\sqrt{6}\, \left(a_2 L_2^2 - a_3 L_3^2\right) y_{2,2}\right], \tag{C10}$$

and for terms of degree 4 ($n = 2$),

$$\begin{aligned} G_{1,2} = \frac{3L_1}{512}\, \Big[& 3\, \left(3 - 30L_1^2 + 35L_1^4\right) x_{4,0} + 2\sqrt{10}\, \left(3 - 21L_1^4 - 6L_2^2 + 2L_1^2\, \left(5 + 7L_2^2\right)\right) x_{4,2} \\ & + \sqrt{70}\, \left(3L_1^4 + L_1^2\, \left(2 - 8L_2^2\right) + 3\, \left(1 - 8L_2^2 + 8L_2^4\right)\right) x_{4,4} + 4\sqrt{10}\, L_2^2\, \left(\left(7L_1^2 - 3\right) y_{4,2} + \sqrt{7}\, \left(6L_2^2 - L_1^2 - 3\right) y_{4,4}\right) \\ & - 12\sqrt{5}\, \left(3 - 10L_1^2 + 7L_1^4\right) z_{4,1} - 4\sqrt{35} L_3^2\, \left(1 + 3L_1^2 - 4L_2^2\right) z_{4,3}\Big] \end{aligned} \tag{C11}$$

$$\begin{aligned} E_{1,2} = & -\frac{2}{\sqrt{5}}\, G_{1,2} + \frac{3L_1}{320}\, \Big[3\sqrt{5}\, \left(-3 + 5L_1^2\right) x_{4,0} + 10\sqrt{2}\, \left(2 - 4L_1^2 + L_2^2\right) x_{4,2} \\ & + 5\sqrt{2}\, \left(-5 + 7L_1^2 + 2L_2^2\right) y_{4,2} + 5\sqrt{7}\, \left(1 + L_1^2 - 4L_2^2\right) (\sqrt{2}(x_{4,4} - y_{4,4}) - z_{4,3}) - 5\, \left(9 - 15L_1^2\right) z_{4,1}\Big] \end{aligned} \tag{C12}$$

$$\begin{aligned} \Delta_{1,2} = G_{1,2} - \frac{3\Delta L_1}{512}\, \Big[& 3a_1\, \left(3 - 30L_1^2 + 35L_1^4\right) x_{4,0} + 2\sqrt{10}\, a_1\, \left(3 - 21L_1^4 - 6L_2^2 + 2L_1^2\, \left(5 + 7L_2^2\right)\right) x_{4,2} \\ & + \sqrt{70}\, a_1\, \left(3L_1^4 + L_1^2\, \left(2 - 8L_2^2\right) + 3\, \left(1 - 8L_2^2 + 8L_2^4\right)\right) x_{4,4} + 4\sqrt{10}\, a_2 L_2^2\, \left(\left(7L_1^2 - 3\right) y_{4,2} + \sqrt{7}\, \left(6L_2^2 - L_1^2 - 3\right) y_{4,4}\right) \\ & - 12\sqrt{5} a_3\, \left(3 - 10L_1^2 + 7L_1^4\right) z_{4,1} - 4\sqrt{35}\, a_3\, L_3^2\, \left(1 + 3L_1^2 - 4L_2^2\right) z_{4,3}\Big]. \end{aligned} \tag{C13}$$

C3 Principal axis limit

In the principal axis rotation mode, when $\hat{\boldsymbol{t}}_3 = \hat{\boldsymbol{b}}_3$, the evolution of mean variables is described by particularly simple equations of motion. Fixing $a_3\Delta = 1$ leads to $S_1 = S_2 = k_3 = 0$, $S_3 = 1$ and $2\, K_3 = \pi$. Then $\dot{\Delta}_3 = 0$, and

$$\dot{G}_3 = -\kappa \sum_{n\geq 1} P_{2n}(0)\, \Theta_{2n}(\cos\varepsilon_3)\, z_{2n,0}, \tag{C14}$$

$$\dot{\varepsilon}_3 = \frac{\kappa}{G} \sum_{n\geq 1} P_{2n}(0)\, \Theta^1_{2n}(\cos\varepsilon_3)\, \left(x_{2n,1} - y_{2n,1}\right). \tag{C15}$$

Table D1. Values of torque coefficients for Eger.

n	m	$x_{n,m}$	$y_{n,m}$	$z_{n,m}$
2	0	0.018 4031	0.0	0.024 9469
2	1	0.002 761 55	−0.017 60 75	0.005 491 36
2	2	0.005 747 53	−0.007 256 87	0.007 602 39
4	0	−0.004 196 57	0.0	0.000 784 584
4	1	0.001 712 36	0.007 247 32	0.001 214 90
4	2	−0.000 738 536	−0.000 386 127	0.004 311 74
4	3	−0.001 128 55	−0.005 660 59	−0.000 244 898
4	4	0.001 025 22	0.001 657 95	−0.001 729 84

Comparison with analogous equations of Breiter & Michalska (2008), which are still simpler than those of Nesvorný and Vokrouhlický (2007, 2008), indicates that most of the effort in earlier works was actually spent on explicitly expressing $\boldsymbol{v}_{n,m}$ in terms of shape harmonic coefficients. The sum on the right-hand side of equation (C14) is equal to $\overline{C}_{0,z}$, and the sum in equation (C15) is $\overline{C}_{1,x} + \overline{D}_{1,y}$ from Scheeres & Mirrahimi (2008).

APPENDIX D: TEST OBJECT: (3103) EGER

The asteroid used in the numerical integration was (3103) Eger. Its convex shape model [see fig. 2 in Breiter & Vokrouhlický (2011)] was obtained by Ďurech et al. (2011) using the light-curve inversion method. The total volume of the asteroid with the given model was $V = 0.418\,879 \times 10^{10}\,\mathrm{m}^3$ which implies an effective diameter of 2 km. Assuming a density $\rho = 2000\,\mathrm{kg\,m}^{-3}$ the shape moments of inertia were $I_1 = 0.245\,025 \times 10^{19}$, $I_2 = 0.518\,318 \times 10^{19}$ and $I_3 = 0.634\,185 \times 10^{19}\,\mathrm{kg\,m}^2$. To speed up the numerical integration of the spin-state evolution we scaled down the asteroid using a factor $s_\mathrm{f} = 0.02$ in every dimension. This means multiplying moments of inertia by a factor s_f^5 and the volume by a factor s_f^3. The dimensionless torque coefficients that were used to compute the YORP torque in semi-analytical theory, calculated from (67) for Eger, are listed in Table D1.

This paper has been typeset from a TEX/LATEX file prepared by the author.